INSTITUTE FOR SUSTAINABLE HERITAGE

MRes SEAHA 2018/2019

Module 5
SEAHA Masters Dissertation

Kathryn Royce Schronk

An investigation of analytical methods applied to mineralogical collection assessment

2nd of September 2019

Assessors: Josep Grau-Bové and Alejandra Albuerne
11850

Table of Contents

Summary

For centuries, mineral collections have been assumed to be stable and inert. However, recent studies have shown that a number of mineral specimens are susceptible to environmental conditions, often leading to chemical and or physical change. These changes require identification and monitoring by analytical methods, lest they become significant enough to be considered as damage by collection stakeholders.

The purpose of this investigation was to assess the applicability of various analytical methods to employ in museums for the study and assessment of mineral collections. Two synthesized sulphate minerals were studied by weight measurements, colorimetry, imaging techniques, and multiple forms of spectroscopy to determine physical and chemical changes resulting from dehydration. While all methods detected change—warranting their use for research applications—colorimetry, photography, x-ray diffraction (XRD), Fourier transform infrared spectroscopy (FT-IR), and Raman spectroscopy were determined to be the most pragmatic techniques at present to use within a museum setting, due to wider availability, cost efficiency, and overall efficacy. However, colorimetry and photography require methodological and technological refinements, and the three spectroscopic methods are not necessarily standalone techniques.

Throughout the investigation, areas for further research were identified. These areas include:

- A comparison of environmental scanning electron microscopy (ESEM) to scanning electron microscopy (SEM) to determine differences in mineral cracking patterns displayed within and without a vacuum.
- An assessment of the usability and applicability of x-ray fluorescence (XRF)—compared to electron dispersive x-ray analysis (EDX)—for mineral collections.
- A study of the rehydration of previously hydrated minerals, to determine if it is possible to reverse the effects of short-term dehydration.
- An experimentation observing the efficacy of Parafilm as a long-term moisture barrier for the storage of environmentally sensitive materials.

These would assess the applicability of additional techniques and potentially produce new treatments for the successful preservation of instable mineral specimens.

This paper was written for submission to *The Geological Curator*; the biannual journal of The Geological Curators' Group (GCG). This publication reaches a large audience of museum professionals, geoscientists, palaeontologists, collectors, and others who frequently handle and care for geological specimens. The results of this investigation are well-aligned with the aims of both the GCG and their journal—to improve the preservation and use of geological specimens—and would be presented directly to those who require this information the most.

Abstract

Two synthetic, hydrated sulphate minerals— melanterite ($FeSO_4 \cdot 7H_2O$) and chalcanthite ($CuSO_4 \cdot 5H_2O$)—were used to assess the applicability of available analytical methods for use in research and collection assessment of mineralogical collections. Weight measurements, colorimetry, photography, x-radiography, computed tomography (CT), scanning electron microscopy (SEM), electron dispersive x-ray analysis (EDX), powder x-ray diffraction (XRD), Fourier transform infrared spectroscopy (FT-IR), and Raman spectroscopy were employed to determine physical and chemical changes induced by the experimental deterioration of the mineral species. Results were compared to naturally occurring specimens at National Museum Cardiff and those presented in the literature. Changes were successfully identified by all methods, but it is inconclusive whether such changes are comparable to those of natural specimens. Of the methods tested, photography, colorimetry, XRD, FT-IR, and Raman spectroscopy were determined to be the most pragmatic for museum applications, due to their wider availability, cost efficiency, and overall efficacy. However, colorimetry and photography require methodological and technological refinements, and the three spectroscopic methods are not necessarily standalone techniques. Further areas of research have been identified to assess the application of additional analytical techniques and to research potential new treatment methods to ensure the preservation of environmentally sensitive minerals.

Introduction

Mineral specimens that have been removed from their geologic origin have been widely assumed to be stable and inert. As such, minerals were often stored in uncontrolled environments, be it a museum basement, closet, shed, or garage. Recent work at National Museum Cardiff (NMC) uncovered a number of mineral species that are susceptible to environmental conditions, including moisture and temperature. Sulphate minerals in particular are largely unstable, for they often have narrow stability fields.

Two such sulphates, melanterite ($FeSO_4 \cdot 7H_2O$) and chalcanthite ($CuSO_4 \cdot 5H_2O$), are the first deterioration products of sulphide minerals such as pyrite (FeS_2) and chalcopyrite ($CuFeS_2$) (Blount 1993, Jambor *et al.* 2000, Chou *et al.* 2013). These hydrated sulphates are often only intermediary deterioration products and will undergo further deterioration (i.e. paragenesis) in the presence of moisture, oxygen, sulphuric acid, and or other mineral species (Jambor *et al.* 2000, Chou *et al.* 2013). Often melanterite and chalcanthite will dehydrate into lower hydrates—such as rozenite ($FeSO_4 \cdot 4H_2O$) and bonattite ($CuSO_4 \cdot 3H_2O$) respectively—before further oxidation or (de)sulfidation occurs (Jambor *et al.* 2000, Chou *et al.* 2013).

Understanding the stability of mineral species, such as melanterite and chalcanthite, within museum environments is important for understanding pyrite's paragenesis within museums as well as for the preservation of unique mineral species. The "rapid rates of hydration, dehydration, and oxidation" (Chou *et al.* 2013: 735) presented by hydrated sulphates challenges the minerals' preservation, yet also lends them perfectly to short-term experimentation.

The principal objective of this study is the assessment of various analytical techniques available. Attempts were made to experimentally degrade samples of melanterite and chalcanthite for up to six weeks to answer the following research questions.

1. Does the short-term dehydration of melanterite and chalcanthite produce chemically or visually detectable change?
2. Do synthetic crystals present changes similar to those observed in museum specimens?
3. What analytical methods are optimal for determining physical and chemical changes to mineral specimens? Which would be most applicable to the average museum, in terms of efficacy and cost benefit?

Background

The environmental stability of melanterite and chalcanthite is affected by the ambient relative humidity (RH) and temperature (Chou *et al.* 2002), so long as the ambient pH is maintained and no additional reactants are present. As temperature and humidity change, so do the minerals' hydration states (Blount 1993, Chou et al 2002, Fig. 1), and quite rapidly as well—sometimes within a day (Chou *et al.* 2013). Supposedly these are reversible changes (Blount 1993, Jambor *et al.* 2000). Yet some museum specimens display irreversible changes. Specimens of melanterite and chalcanthite at NMC have extensively deteriorated over decades of storage, now exhibiting a changed appearance and a suspected altered composition. These changes are problematic for stakeholders as they equate to damage: the unacceptable degradation of value-defining aspects caused by agents of deterioration (Royce & Baars *in preparation*). For minerals and other geological materials, their physical integrity is vital to their value, as their aesthetic, monetary, display, and research values can change dramatically with physical and chemical alterations (Cotterell 2019). These changes can in turn lead to loss of information and previous uses, turning a once priceless specimen into a useless one.

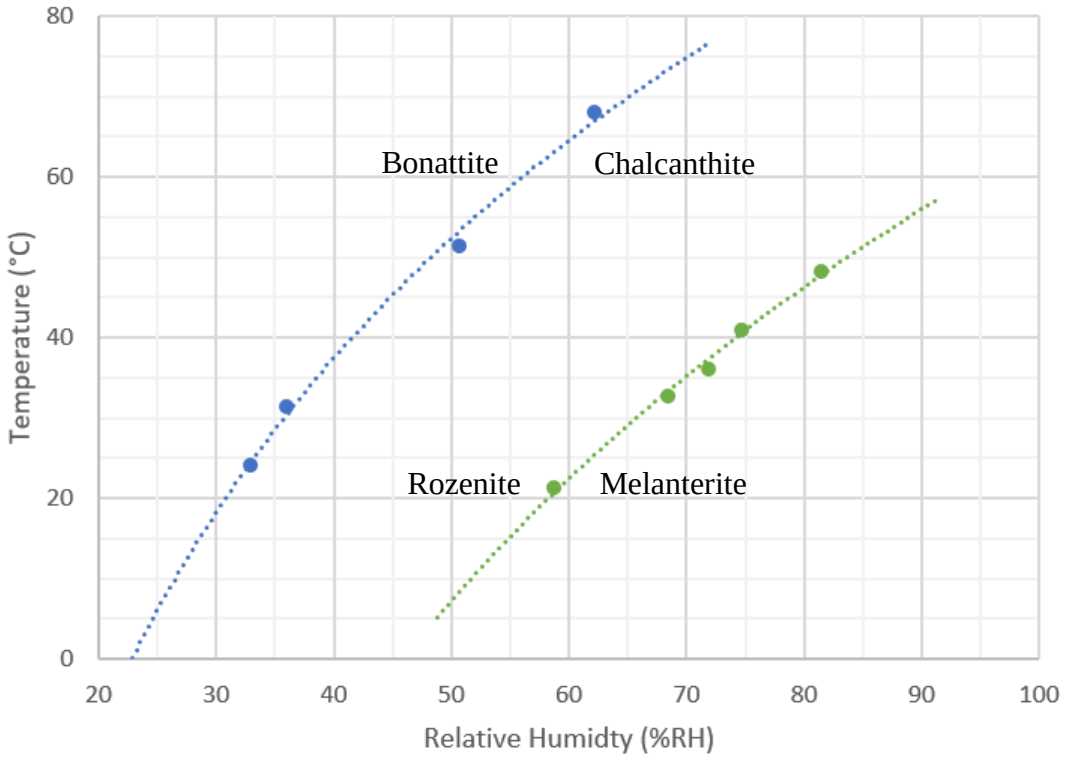

Figure 1. The reported temperature and RH equilibrium for chalcanthite-bonattite & melanterite-rozenite transitions (after Chou et al. 2002).

Methodology

Melanterite and chalcanthite crystals were grown from reagent grade chemicals via the evaporation of a super-saturated solution. These crystals were then divided into sample and control groups, with the former placed into an environmental chamber and the latter into a simulated, minimally controlled storage environment. Selected samples, controls, and seed crystals were analysed by various techniques, including weight measurements, colorimetry, imaging, and spectroscopy.

Crystal Growth

Whilst chemical variations are expected in natural specimens, they can affect the products of a reaction, adding uncertainty and discontinuity to experimental results. Thus, pure compositions were desired for this experiment and were laboratory-grown to reduce compositional variables. Chalcanthite was grown from ≥99.0% copper(II) sulphate pentahydrate (Sigma-Aldrich) and deionized water. Melanterite crystals were grown from 98% iron(II) sulphate heptahydrate (Alfa Aesar), 0.2N sulphuric acid (standardised solution; Alfa Aesar), and deionized water. Sulphuric acid was added to the iron solution to halt Fe^{2+} conversion to Fe^{3+} by reducing the solution's pH, allowing for larger melanterite crystals to grow. See Appendix A for further details.

Dehydration

Experimental Samples

To encourage dehydration, samples of chalcanthite and melanterite were exposed to 35% RH at 30°C. At these conditions, dehydration is likely to occur (Fig. 1). The RH is also representative of a conditioned museum environment.

Ten chalcanthite samples were exposed for 45 days, whilst five melanterite samples were exposed for 28 days. The difference in time was due to difficulty in growing a sufficient number of melanterite crystals, which was not reached until two weeks into the experiment.

The samples were placed within 41ml 'Mason' glass jars without lids. Conditions were maintained by the use of the Binder APT KBF115 environmental chamber. To confirm temperature and RH, two iButton hygrochron temperature and humidity loggers (DS1923; Maxim Integrated) were used. The chamber was checked 2–3 times per week to ensure conditions were maintained. The exterior chamber door was also opened briefly each week to monitor deterioration progress; the samples were left undisturbed.

Control Samples

The controls were 'stored' in a laboratory cupboard, replicating a dark storage environment with ambient conditions. Ten chalcanthites were exposed for 45 days, and four melanterites were exposed for 28 days. Controls were stored in 41ml 'Mason' glass jars, covered with Parafilm M (Bemis PM-996), then sealed with an enamelled metal lid.

Analytical Methods

Analytical methods were performed before and after experimentation to determine changes induced by dehydration. Surplus seed crystals were used for pre-deterioration analysis with the scanning electron microscope (SEM) and the various spectroscopic techniques. All other methods were performed with the samples and controls. Powder x-ray

diffraction (XRD) was also performed on selected specimens from NMC to anticipate and compare the dehydration products of the synthesized minerals to those of naturally occurring specimens.

Weight Measurements

Samples were weighed with an A&D Company Limited HR-100AZ high precision balance, which has an accuracy of ±0.1mg. The average of three measurements was taken.

Colorimetry

A Konica Minolta CM-700d spectrophotometer was used to measure changes in mineral colour before and after experimentation. A pulsed xenon lamp with UV cut filter, replicating a D65 CIE illuminant with the wavelengths of 400-700nm, was used to expose a 3mm reading area to both specular and diffused reflected light. This was detected by a silicon photodiode array. White and black calibration occurred prior to each reading using the equipment's associated standards. The values recorded were the average measure of three readings.

Imaging

Photographs were used to visually determine macroscopic changes. A Canon PowerShot SX40HS point and shoot camera was used in 'Manual' mode, with an f-stop of f/8, ISO 100, and shutter speed of 1/50sec. Images were colour balanced against a 50% grey colour card (included in each image) in Adobe Lightroom.

Computed tomography (CT) was used to identify structural, surface, and volumetric changes, whilst x-radiographs visualised internal growth boundaries and imperfections. Pre- and post-experimental CT data was overlaid to compare variations induced by dehydration. Scanning and data manipulation was provided by OR3D through the use of the RX Solutions Desk Tom CT scanner with Volume Graphic's software, VGSTUDIOMAX.

A Jeol 5910 SEM was used at 10kV and 1nA to microscopically view crystal surfaces, cracking patterns, and other signs of deterioration such as efflorescence.

Spectroscopy

Electron dispersive x-ray analysis (EDX) provided elemental analysis. An Oxford Instruments INCA 300—attached to the above SEM—acquired spectra at 15kV and 1nA.

Powder XRD was used to identify the minerals' crystalline structure. A PANalytical Xpert-Pro diffractometer with a Cu anode was used to continuously scan rotating powdered samples at 40kV and 30mA. Spectra were acquired over the range of 5-70°2Θ, with each step (0.02°) being scanned for 38 seconds. The resultant spectra were compared to those within the International Center for Diffraction Data's (ICDD) Powder Diffraction File (PDF).

Infrared and Raman spectroscopy were used for compound analysis, particularly in the identification of alterations in hydration state. A Perkin Elmer Spectrum 100 Fourier transform infrared spectrometer (FT-IR) with an attenuated total reflectance (ATR) accessory was used to analyse powdered samples over the range of 4000-520cm^{-1}. A Renishaw inVia confocal Raman microscope with a 514nm laser acquired spectra from the same powder samples from 3800 to 100cm^{-1}. Spectra from both methods were compared with those recorded in the literature.

Results

Crystal Growth

Twenty chalcanthite specimens were grown, averaging 34 x 23 x 16 mm, whereas nine melanterite crystals were successfully grown, averaging 22 x 17 x 7 mm.

Chalcanthite crystals were simple and quick to grow, often only requiring three days to produce those of the size aforementioned. The process is straightforward (Appendix A) and produces exemplary specimens. The melanterite, on the other hand, proved more elusive and difficult to produce sufficiently large crystals. The procedure outlined in Appendix A is the product of many rounds of trial and error, which consisted of three batches of super-saturated solution and their resultant crystals. Each batch varied slightly from the other, most notably in the colour of both the solution and its crystals. The first attempt produced a bright rusty orange solution and bottle-green crystals (M1-3). The second and third solutions were sour apple and olive green, respectively. Both produced aqua crystals (M4-6 and M7-9, respectively).

Dehydration

Throughout the duration of the experiment, the chalcanthite samples showed no visual signs of dehydration, such as discolouration, efflorescence, or the development of a powdery surface. Yet within four days of exposure to experimental conditions, the melanterite samples had superficially dehydrated, turning an opaque, powdery pale green. After four weeks' exposure, it was thought likely that these samples had dehydrated throughout. This was soon confirmed when M5 and M9 broke during handling after photography and colorimetry respectively.

As for the controls, both those of chalcanthite and melanterite showed no visual signs of deterioration, suggesting that sealing containers with Parafilm is successful at retaining moisture.

Analysis

Weight measurements

The accuracy of the balance is reported as ± 0.1mg (or ± 0.0001g). All samples and controls displayed changes outside of this range (Table 1). All—save M9—lost weight, signifying some degree of water loss. M9 was the only one to gain weight.

There is a marked difference in the weight lost between the melanterite samples (>10%) and their controls (<0.25%). This can be classified as meaningful change. The same cannot be said for the chalcanthites as the amount of weight lost by both the samples and controls is less than 2% of their initial weight, with a majority losing <0.5%. Only three samples—C4, C5, and C10—lost more than 1% of their original weight.

Table 1. Average weights of the melanterite and chalcanthite crystals before and after dehydration with the change in weight presented in grams & percentage.

		Sample #	Average Weight Before Dehydration (g)	Average Weight After Dehydration (g)	Δ Weight (g)	Δ Weight (%)
Melanterite	Sample	M1	3.7659	1.4372	-2.3287	61.84%
		M3	3.3439	2.9905	-0.3533	10.57%
		M5	2.4133	1.7498	-0.6635	27.49%
		M7	3.3785	2.5274	-0.8511	25.19%
		M9	2.4862	2.8218	+0.3356	13.50%
	Control	M2	4.0689	4.0644	-0.0045	0.11%
		M4	2.9228	2.9172	-0.0056	0.19%
		M6	2.1616	2.1565	-0.0051	0.24%
		M8	2.1062	2.1025	-0.0037	0.17%
Chalcanthite	Sample	C1	8.0082	7.9874	-0.0208	0.26%
		C2	7.0555	6.9981	-0.0574	0.81%
		C3	8.1657	8.1167	-0.0490	0.60%
		C4	15.8713	15.5747	-0.2965	1.87%
		C5	12.1782	12.0552	-0.1230	1.01%
		C6	9.6042	9.5149	-0.0893	0.93%
		C7	9.9183	9.8605	-0.0578	0.58%
		C8	19.6154	19.5263	-0.0891	0.45%
		C9	11.5087	11.4282	-0.0805	0.70%
		C10	12.5707	12.4205	-0.1502	1.20%
	Control	C11	17.2549	17.0894	-0.1654	0.96%
		C12	5.1727	5.1650	-0.0077	0.15%
		C13	7.6671	7.6450	-0.0221	0.29%
		C14	7.5042	7.4902	-0.0140	0.19%
		C15	5.0408	5.0061	-0.0346	0.71%
		C16	6.6649	6.6447	-0.0201	0.30%
		C17	7.0838	7.0804	-0.0034	0.05%
		C18	7.1677	7.1533	-0.0144	0.20%
		C19	4.7220	4.7056	-0.0164	0.35%
		C20	7.4641	7.4055	-0.0586	0.78%

Colorimetry

Each crystal was analysed before and after the experiment. Lightness and chroma values, chromaticity coordinates, and hue angles were calculated for each measurement by Konica Minolta's SpectraMagic NX software associated with the device.

Two sets of values were produced; one with the specular component included (SCI) and the other with it excluded (SCE). SCI measurements give values for an object's 'true' colour, unaffected by surface features such as gloss or roughness (Konica Minolta 2019). This is not how humans perceive an object's colour, however. The exclusion of specular reflected light allows for the detector to act more like the human retina, increasing sensitivity to surface conditions (Konica Minolta 2019). This is ideal for conservation applications, where it is necessary to mitigate changes to an object's perceived colour. The values reported here and in Appendix B are thus SCE measurements in order to relate the data to visual observations.

The 1976 CIE L*a*b* colour space was chosen for its simplicity and ubiquity (Johnston-Feller 2001, Konica Minolta 2007). L* is the value attributed to lightness on a scale from -100 (black) to 100 (white). a* is a chromaticity value attributed to a red-green

axis where positive values are red and negative values are green. b* is the yellow-blue axis with positive values being yellow, negative values being blue. Both a* and b* scale from -60 to 60.

Johnston-Feller admits that "any unit of color difference can be helpful in describing the relationship between similar colors," (2001: 33) yet the total colour change (ΔE^*_{ab}) is useful for discussing the distance between before and after values within the L*a*b* colour space. To determine ΔE^*_{ab}, one begins by determining the changes(Δ) in L*, a*, and b* by subtracting the averaged before value from the averaged after value (Eq. 1, using L* as an example).

$$\Delta L^* = L^*_{aft} - L^*_{bef} \quad (1)$$

These values are then entered into the 1976 CIE L*a*b* equation (Eq. 2) to determine the total colour change from before to after of a single sample.

$$\Delta E^*_{ab} = \sqrt{(\Delta L)^2 + (\Delta a)^2 + (\Delta b)^2} \quad (2)$$

As a whole, the chalcanthites remained within the same colour space after the experiment as they did prior to it (Appendix B). All had positive, whiter L* values and negative, blue b* values. a* values sat more or less equally on either side of 0, with values between ±9. The ranges were larger than anticipated, however, as all crystals visually appeared more or less the same colour. This is likely attributed to poor contact between the meter and the crystals, due to the lack of sufficiently large, even crystal surfaces for the meter to rest upon. The poor contact, in addition to the crystals' transparency, likely allowed for additional, external light to reach the detector and skew the recorded values.

When reviewing each crystal's colour change, there is great variation across all values (Table 2). No obvious trend is apparent; neither the samples nor the controls moved together in the same direction for any specular component. Nor did the samples see a significant change relative to the controls. In fact, there is no computed difference between them. The near randomness of the spread suggests that values within these ranges are discrepancies resulting from external variables. Thus, it cannot be said with certainty whether any of these crystals changed colour, as there is no correlation between visual observations and the numerical values calculated.

Table 2. ΔL, Δa*, Δb*, and ΔE*$_{ab}$ values for the chalcanthite minerals with associated descriptive statistics.*

		ΔL*(D65)	Δa*(D65)	Δb*(D65)	ΔE*$_{ab}$(D65)
Samples	C1	-9.94	2.46	-0.87	10.27
	C2	-0.97	0.51	-2.11	2.38
	C3	7.55	-3.12	1.33	8.28
	C4	4.77	-2.42	-5.04	7.35
	C5	-4.89	3.84	-5.02	7.99
	C6	-2.49	-0.45	-1.93	3.18
	C7	9.75	-5.38	4.25	11.92
	C8	6.83	-9.07	-12.64	16.99
	C9	-0.94	-9.16	-16.20	18.64
	C10	-1.43	2.67	-3.79	4.85
	Mean	0.82	-2.01	-4.20	9.19
	Standard Deviation	5.89	4.46	5.83	5.16
Controls	C11	1.03	0.50	-0.98	1.51
	C12	2.67	-5.57	-4.68	7.75
	C13	-2.56	-0.86	1.33	3.01
	C14	-5.64	4.22	10.41	12.57
	C15	-0.12	-0.22	0.81	0.85
	C16	5.53	-0.71	9.11	10.68
	C17	2.75	0.04	-2.84	3.96
	C18	7.96	-1.95	-2.55	8.58
	C19	8.48	-0.70	2.89	8.99
	C20	-12.21	-2.24	-18.53	22.31
	Mean	0.79	-0.75	-0.50	8.02
	Standard Deviation	6.02	2.33	7.62	6.07

The melanterite samples, however, did experience a significant colour change, largely becoming lighter than they were prior to the experiment (Table 3). All five melanterite samples had a $\Delta E^*_{ab} > 56.50$, whereas the controls had a $\Delta E^*_{ab} < 19.00$. While all samples saw significant changes in ΔL*, the changes in a* and b* are less obvious. Although M6 has a larger ΔL* compared to the other controls, both its ΔL and ΔE^*_{ab} are significantly smaller than those of the melanterite samples. While it is possible that M6 did darken some, it is likely not to a noticeable degree and cannot be confirmed visually.

Table 3. ΔL, Δa*, Δb*, and ΔE*$_{ab}$ values for the melanterite minerals with associated descriptive statistics.*

		ΔL*(D65)	Δa*(D65)	Δb*(D65)	ΔE*$_{ab}$(D65)
Samples	M1	57.18	5.87	10.53	58.43
	M3	57.70	3.29	2.60	57.85
	M5	56.16	9.20	2.23	56.96
	M7	62.39	10.84	4.76	63.51
	M9	57.88	7.73	-0.72	58.40
	Mean	58.26	7.39	3.88	59.03
	Standard Deviation	2.15	2.62	3.76	2.30
Controls	M2	-1.20	1.46	-3.27	3.78
	M4	3.96	-2.15	-0.07	4.50
	M6	-18.34	-0.52	1.16	18.38
	M8	-4.47	6.32	1.55	7.90
	Mean	-5.01	1.28	-0.16	8.64
	Standard Deviation	8.26	3.18	1.89	5.83

Imaging

Photography

Photography of all minerals occurred before and after the experiment with the same lighting and equipment. The one thing that did change, however, was the positioning of the minerals. This variation did produce a noticeable difference; the minerals in the before photos often look much glossier than those in the after photos (Fig. 2). Even slight differences in their resting positions varies the reflectance angle of the light, sometimes causing glare.

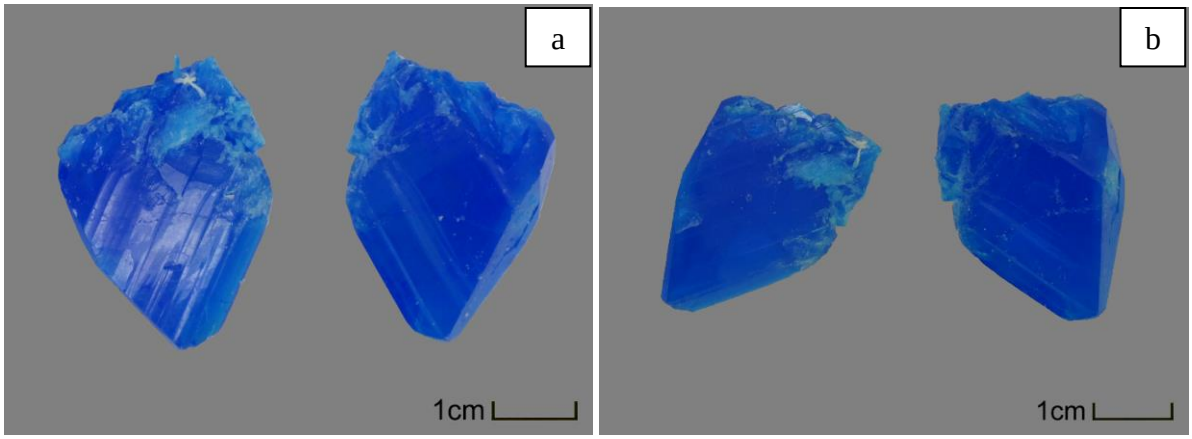

Figure 2. Photographs of C16 a.) before (obverse and reverse), and b.) after (obverse and reverse) the experiment. Note the lack of glare to the mineral in b. This is attributed to a slight variation in the position of the mineral for photography, causing the light to reflect differently off its surface.

X-radiography

X-radiographs were captured for samples C8, M1, and M3 and controls C12, C18, and M2. The following images are read in the opposite manner of traditional x-rays; whiter areas are less dense, and vice versa. Also, the grey scales are not comparable between radiographs, and the densities are relative to that particular radiograph.

While it would be ideal to compare densities across all radiographs and all crystals, this was not the intent of employing the technique. Rather, it was used to view the crystals' internal features. To this end, the technique was successful, highlighting crystallization boundaries, chips, voids, and other imperfections. C8 (Fig. 3) is a good example to view many such imperfections. Most notable is the fine gap between the upper and base crystals, which was not apparent whilst handling the sample. The striation across the sample, most notable in the upper crystal, represents growth boundaries.

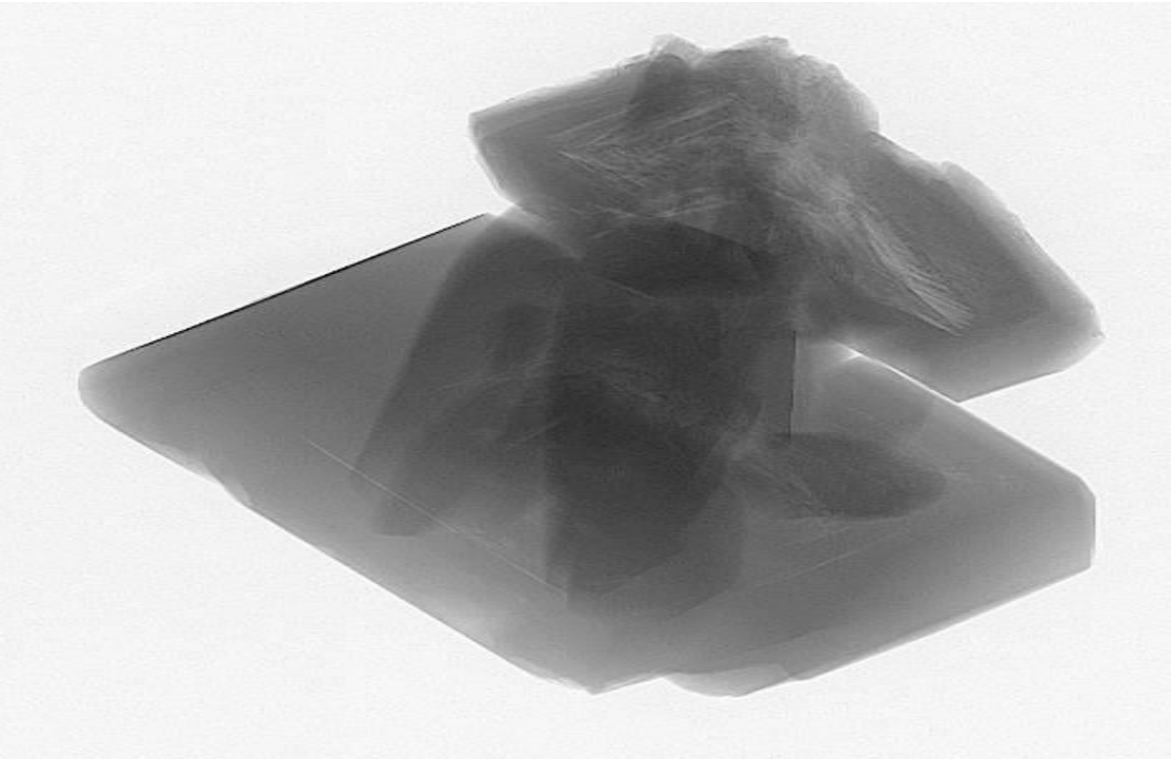

Figure 3. X-radiograph of C8 depicting multiple growth boundaries.

M1 (Fig. 4) displays similar imperfections. The crack running from the upper right-hand corner to the lower left-hand corner is the most prominent feature. It existed prior to exposure (Fig. 4a) —most likely forming during the crystal's growth—yet widened and became more distinguishable after dehydration (Fig. 4c). This crack runs through the entire depth of the crystal, as it has distinct internal plane visible in the images (Fig. 4a-b.

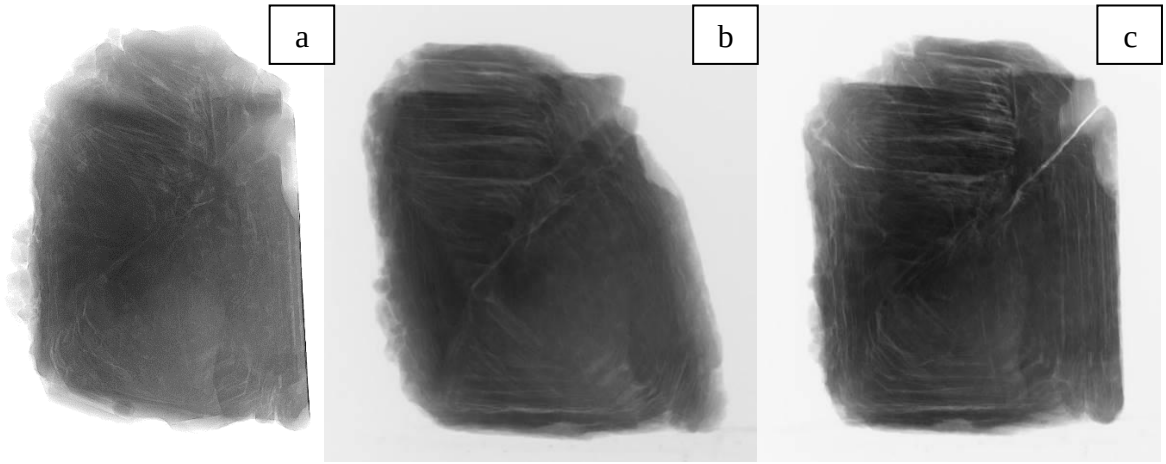

Figure 4. X-radiographs of M1 a.) before and b-c.) after dehydration. Key features are the angular, concentric growth boundaries and the cracks in the crystal's upper portion. Both before and after (a-b), it is possible to distinguish a distinct, internal plane at the upper right-hand corner which indicates that the crack runs through the depth of the mineral.

Many features are the same between before (Fig. 4a) and after (Fig. 4b-c), yet they appear more distinct, especially the angular, concentric lines of the growth boundaries. One difference, however, is the propagation of the crack in upper left-hand corner (Fig. 4c) along what was probably originally one such growth boundary.

CT

Two melanterites (M1-2) and two chalcanthites (C8 and C18) were scanned before and after the experiment. Two-dimensional slices for each axis (x, y, and z) as well as a three-dimensional model were produced for each mineral for both scans. The 3D models of the before and after scans were then overlaid to provide a direct comparison. M1 was the only one to see significant changes.

Comparing M1's before and after slices (Fig. 5), many of the previous internal features have become more distinguishable with dehydration, new features have developed, and the external edges have been eaten away. In particular, the crack at lower right-hand corner and the central voids have become larger and better defined. New areas of lower density at the crystal's edges and left-hand side have developed as well and seem to connect the voids and cracks along preferential crystal planes.

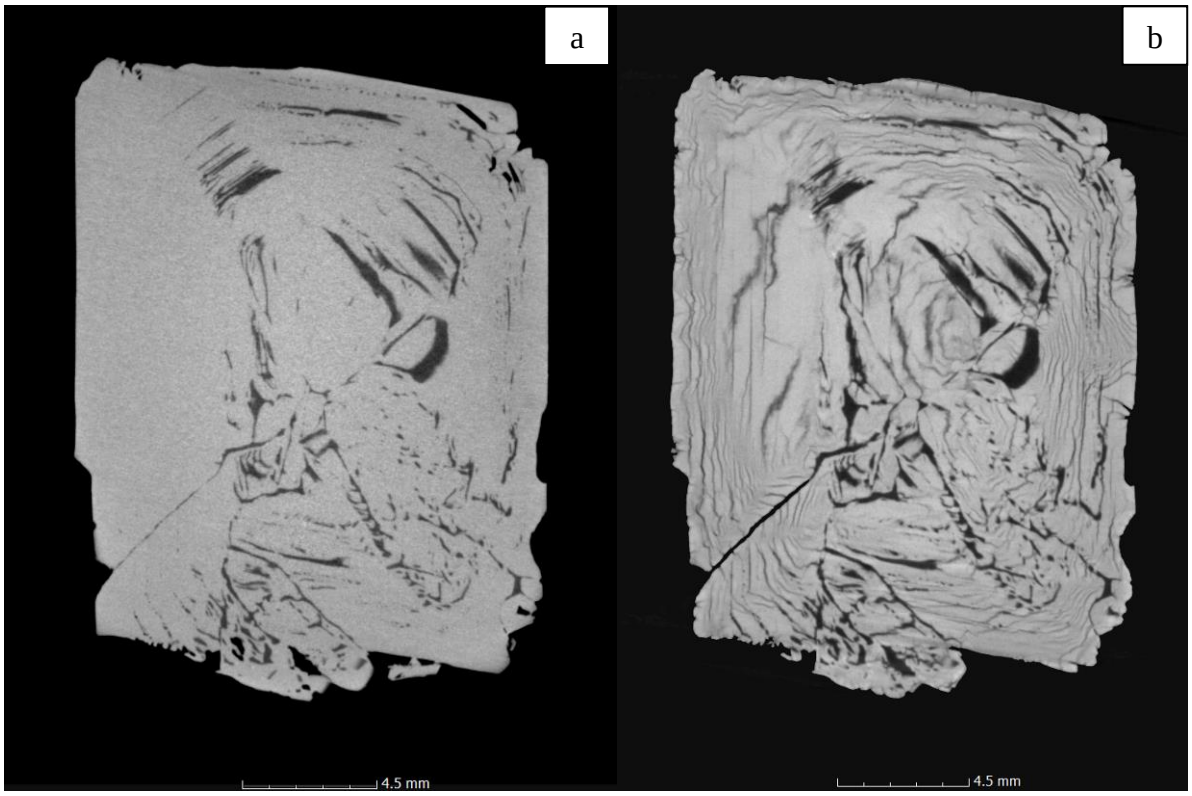

Figure 5. CT slices of M1 a.) before and b.) after dehydration, depicting the extent of change that resulted. Most notable is the development of features on the left-hand side and the development of the large crack in the lower left-hand corner.

The other crystals, however, depict very little variation to internal features between the before and after slices (Fig. 6). Yet they still provide information about the crystals' structures, as one is able to see the angular growth boundaries, some fine cracks, and voids.

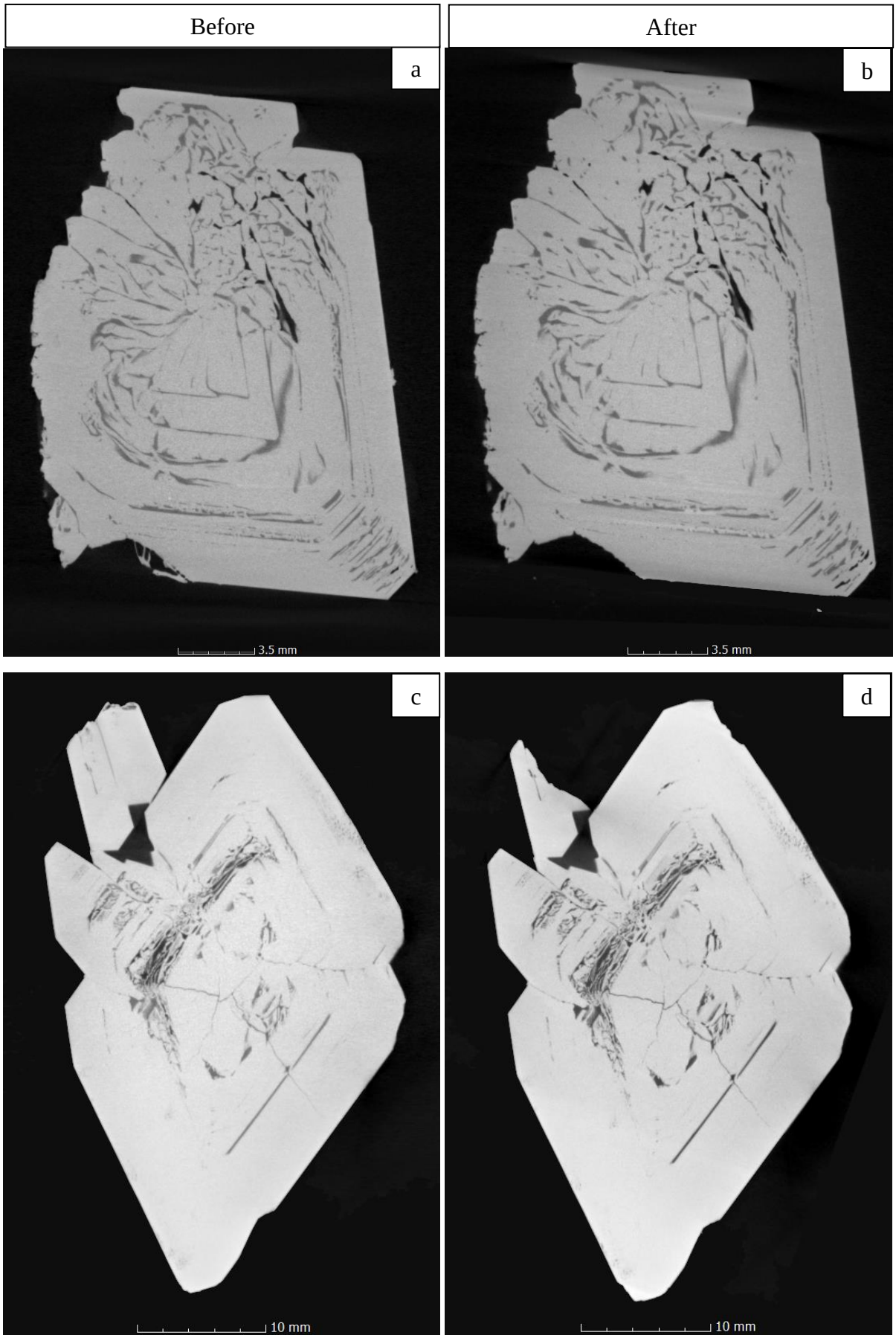

Figure 6. CT slices show that there is very little variation between M2 (a & b) and C8's (c & d) before and after. The part missing from C8 in the upper left-hand corner of d) is part of the crystal that broke off during transportation after the experiment.

Turning to the 3D overlaid models, one quickly notices the extent of change undergone by M1. Most of its original surface has been lost (Fig. 7), and star-like pores with radiating cracks have emerged on the sides (Fig. 7d) and front (Fig. 7a) post-dehydration.

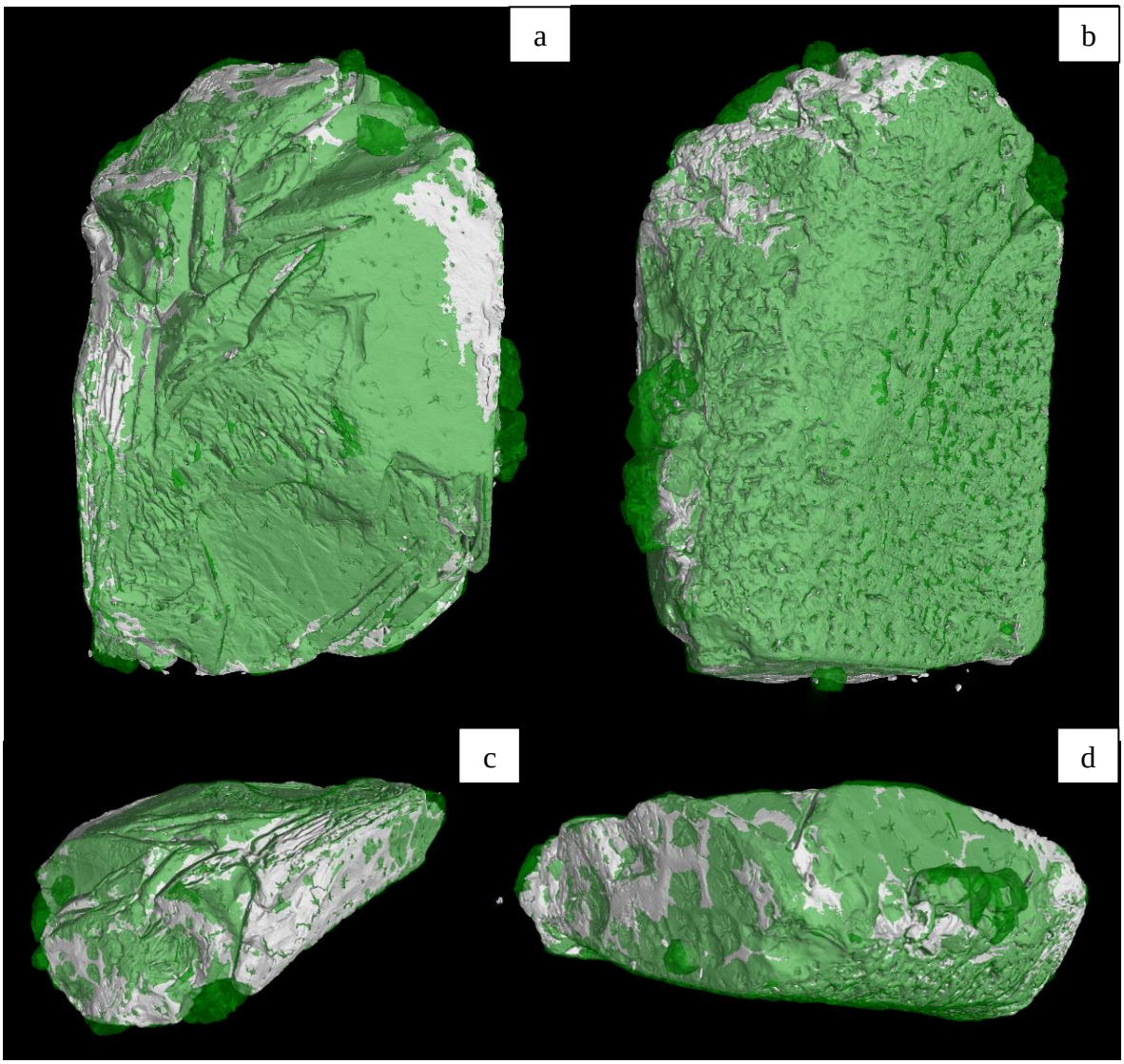

Figure 7. A 3D render of M1, depicting the amount of surface lost from various angles. Green areas show the original, pre-dehydration surface, whereas the white shows the present surface that matches the original's. The darker the green, the more extensive the loss.

For the other crystals scanned, most losses occurred at crystal points and edges (Fig. 8); areas which are prone to damage from physical stress (ex. handling or transportation). The losses seen on these crystals appear to be the result of such stresses rather than chemical reaction, as the breakages are localised and small relative to the whole crystal.

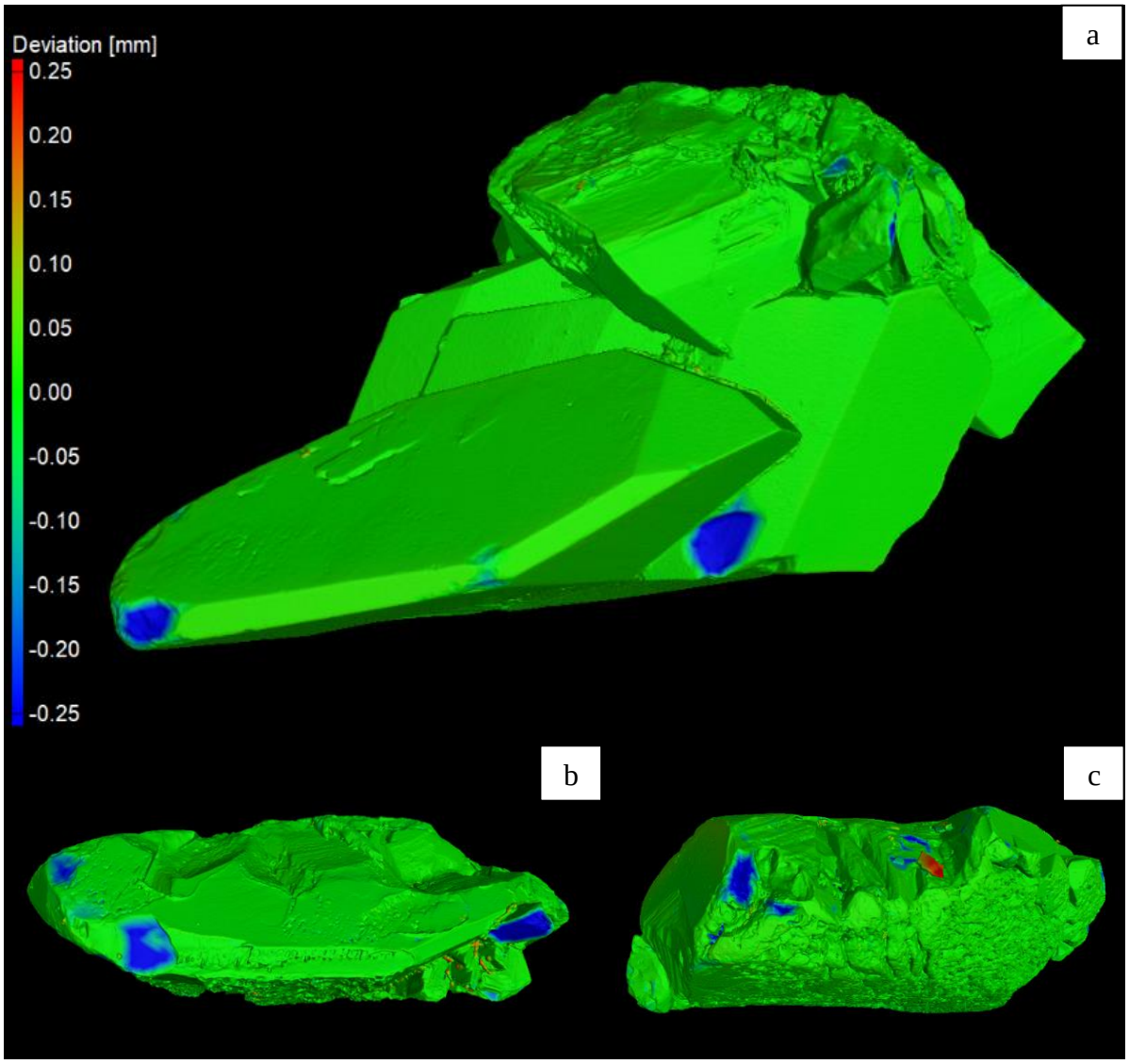

Figure 8. Colour maps depicting surface deviations of the post-dehydration crystal—a.) C8, b.) C18, c.) M2—to its original form. Blue areas show loss, while green areas show little or no deviation.

SEM

Seed crystals of both minerals and samples from C7, C10, C14, and M5-7 (Fig. 9) were observed. The most notable microscopic difference between chalcanthite and melanterite is the cracking patterns, likely attributable to their different crystalline systems (Appendix A). However, these cracks were likely induced by the evacuation of water from the samples during the establishment of a vacuum within the SEM's chamber. Consequently, there is uncertainty of how representative these cracks are of slowly—rather than rapidly—dehydrated samples.

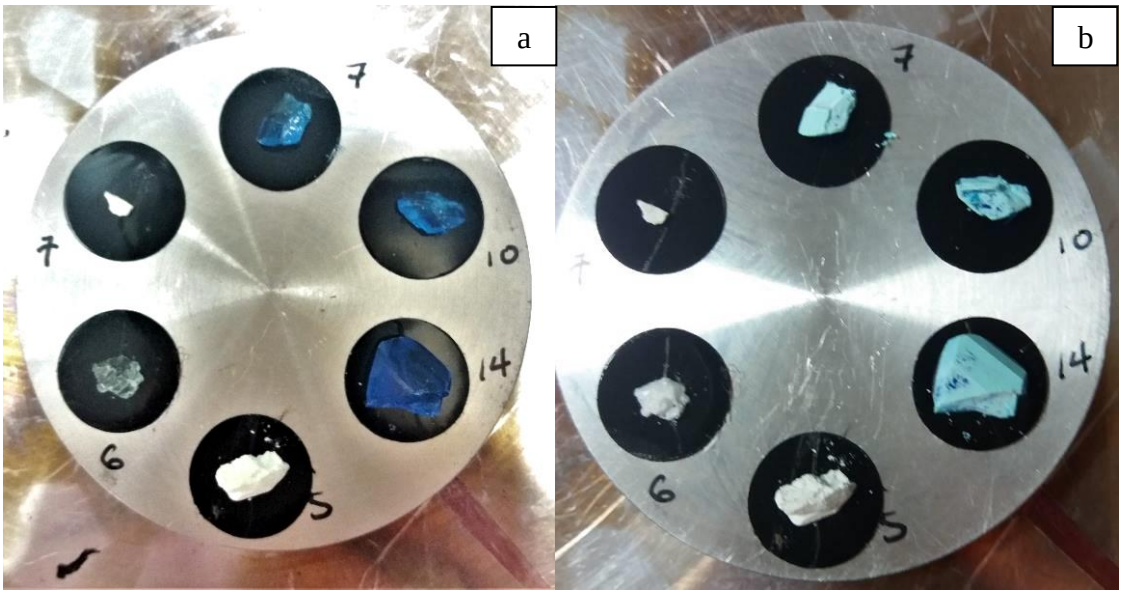

Figure 9. Samples a.) before and b.) after SEM observation. The establishment of a vacuum within the SEM chamber rapidly dehydrated the samples to a lower hydrate or anhydrous phase, as indicated by their changed appearance.

Melanterite

Melanterite has a fairly uniform surface with no distinct macroscopic features (Fig. 10a). It is not until it is viewed at higher magnifications that a wavy, flaky pattern of fissures begins to emerge (Fig. 10b-d). This pattern is reminiscent of overlapping keratin scales. One can also see a striated surface of parallel microcracks at higher magnifications (Fig. 10c). These microcracks are perpendicular to the fissures, suggesting preferential planes of deformation. Cracks propagate along both planes, moving across the surface in a stepwise fashion (Fig. 10d). This cracking pattern suggests that melanterite is likely to exfoliate, with fragments breaking from the body once sufficiently deep fissures and cracks intersect.

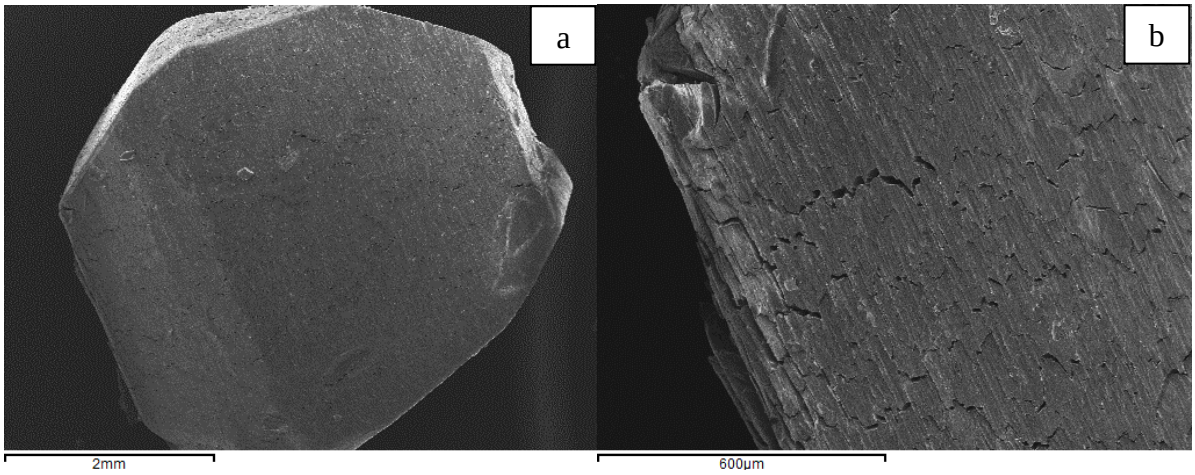

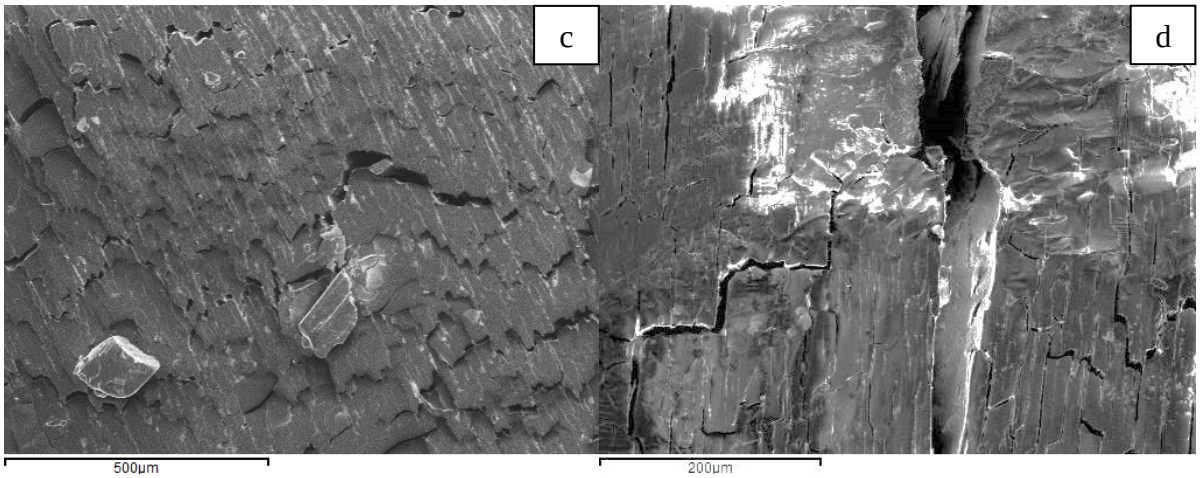

Figure 10. SEM micrographs of melanterite at increasing magnifications; a-c) are images of a seed crystal, whilst d.) is a sample taken from M6. At higher magnifications, the fissures, microcracks, and the stepwise pattern of crack propagation (d) become more distinct.

The samples from M5 and M7 have a markedly different surface; uneven and powdery (Fig. 11a). Cracks and pores are distinct (Fig. 11b), often forming star-like shapes. At higher magnifications (Fig. 11c), a series of winding cracks and fractures begins to emerge, which in time would likely both lengthen and widen. This extensivity of cracking allows for exfoliation of small fragments to occur when exposed to mild stresses, such as handling or transportation.

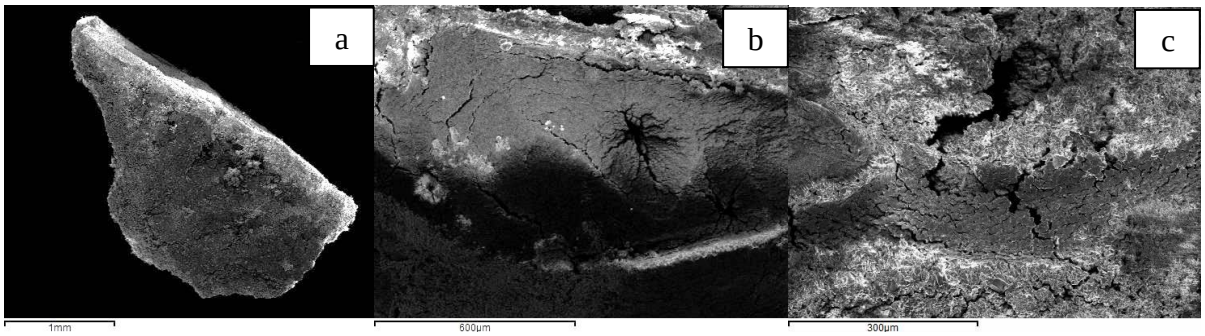

Figure 11. SEM micrographs depicting the uneven, powdered surface of dehydrated melanterite (M7). The most notable features are a.) its macroscopic fuzzy appearance, b.) star-shaped pores with radiating cracks, and c.) a winding cracking pattern which appears at higher magnifications.

Chalcanthite

Macroscopically, it is possible to discern concentric 'ellipses' in the centre of and some striation on the seed crystal in Figure 12a. These are the effects of microcracks (Fig. 12b). The cracks appear to originate from a point and grow in two directions producing a 60°:180° intersection (Fig. 12c). Cracks seem to propagate when those of two adjacent points meet, so that a larger crack is the assembly of multiple 'X'-shaped origins aligned in one direction. However, in some instances, rather than producing one long crack with multiple microcracks coming off from it (Fig. 12c), the cracks can propagate in three or more direction from the origin, producing a basket-wave pattern (Fig. 12d)

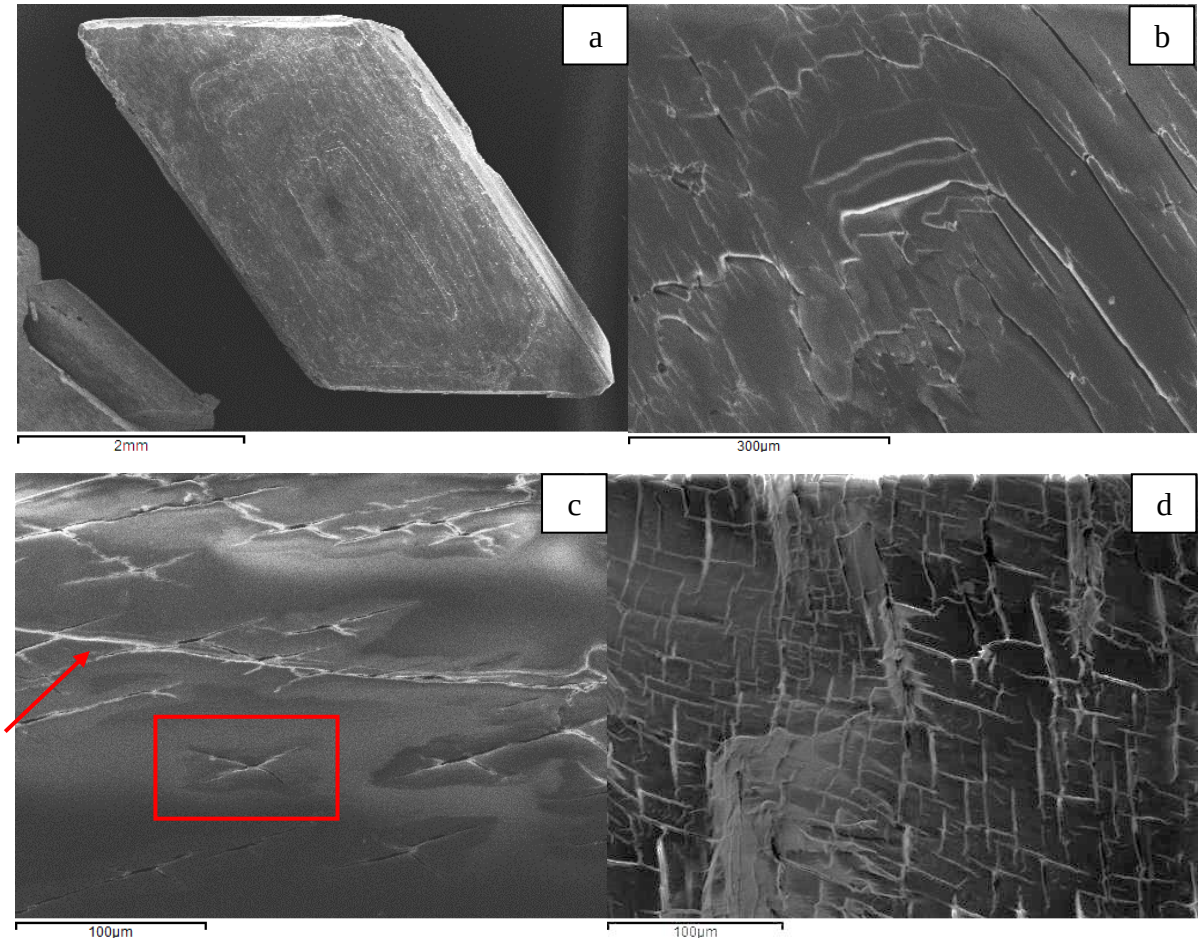

Figure 12. SEM micrographs of chalcanthite of increasing magnification. At higher magnifications, the cracks and their origins become more distinct (highlighted by rectangle in c). Cracks will propagate either in one long line (highlighted by arrow in c) or in a basket-weave pattern (d).

The sides of the chalcanthite crystals are not always flat, also being rough or ridged (Fig. 13). These seem to be created from cracking, breakages, or the termination of the crystalline structure. Situated among these ridges can be pores of varying sizes. While they do not seem to be the origin of cracks, they still pose a threat to the mineral's stability by increasing the number of potential reaction sites.

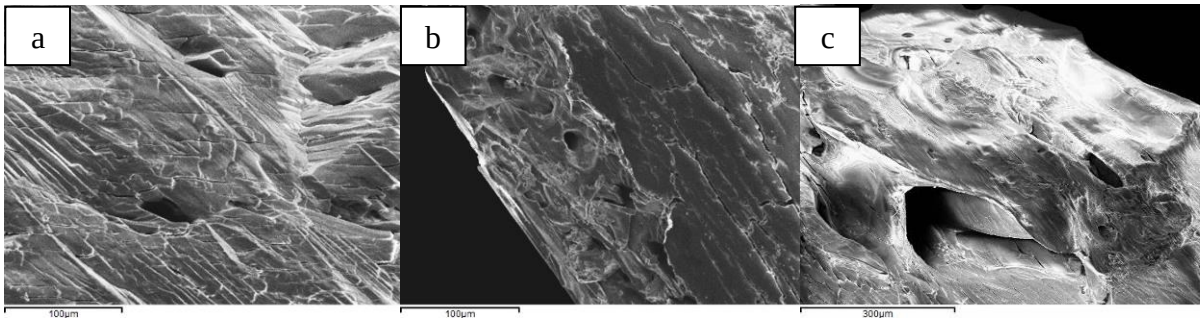

Figure 13. SEM micrographs depicting examples of pores found at the edges of chalcanthite seed crystals (a-b) and C10 (c).

Spectroscopy

EDX

Four to ten spectra were taken at various locations across the samples used for SEM analysis. In each spectrum, the peak positions remained the same, with only the magnitude varying. All of the peaks' heights moved relative to one another; in other words, no one element's peaks varied significantly or by itself to suggest a higher proportion of that element in a given location. Thus, the variation seen is likely due to the topography of the spectra's locations, with certain locations providing an optimal angle to return a higher proportion of the x-ray beam to the detector. No additional elements were detected (Fig. 14), evidencing their compositional purity.

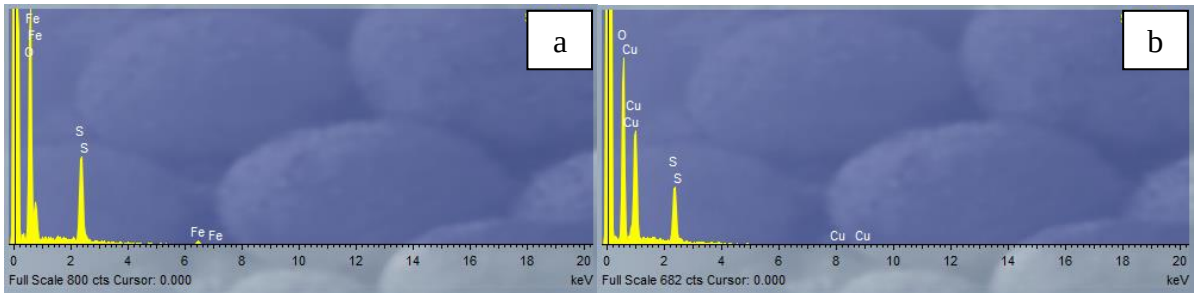

Figure 14. Representative EDX spectrum of a.) melanterite and b.) chalcanthite.

XRD

Powdered samples from ten synthetic crystals (Table 4) and seven museum specimens from NMC (Table 5) were analysed and their spectra compared to those within the Powder Diffraction File.

Synthetic crystals

Four chalcanthites and six melanterites were sampled and analysed (Table 4).

Table 4. XRD results of the synthetic crystals.

Mineral	Sample	XRD Results
Chalcanthite	seed crystal	chalcanthite
	loose flakes from mixed samples	chalcanthite
	C2	chalcanthite
	C11	chalcanthite
Melanterite	batch 1 seed crystal	melanterite
	batch 2 seed crystal	melanterite
	batch 3 seed crystal	melanterite
	M5	rozenite
	M7 surface product	rozenite, melanterite, szomolnokite
	M6	melanterite

The pattern presented by the four chalcanthite spectra (Fig. 15) are consistent and well-matched, both amongst each other and to reference spectra. The variations between spectra are minor and are chiefly limited to differences in magnitude. There is occasional broadening of some peaks, most notably that at 22-24°2Θ, but the peak positions are retained.

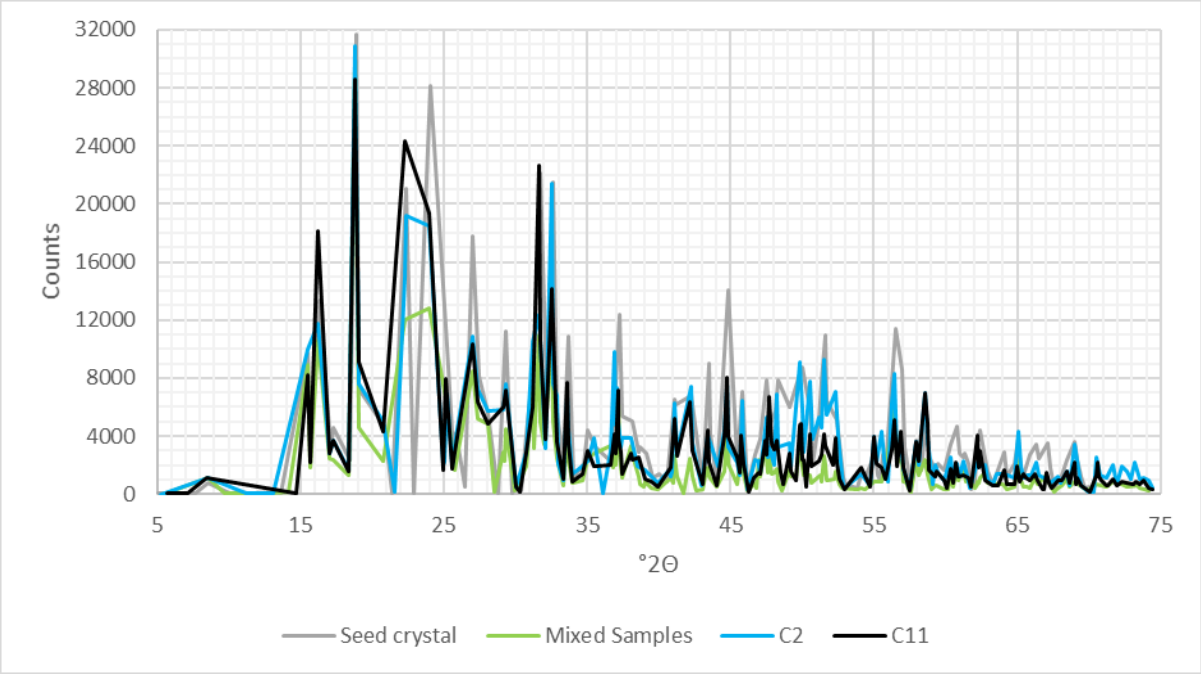

Figure 15. XRD spectra of a chalcanthite seed crystal, mixed samples, C2, and C11. These four profiles are fairly well matched to each other and the chalcanthite reference spectra.

Three different melanterite seed crystals were analysed to determine if there were any structural differences between the melanterites produced by the various solutions. Whilst there are some minor variations in magnitude and peak breadth between batch one's seed crystal and those of the other two batches, the spectra share the same profile (Fig. 16) and match melanterite reference spectra. M6 also matches this pattern. These four spectra share a very strong peak at 18.1°2Θ, with other major peaks shared at 23.6, 27.4, 34.2, and 48.8°2Θ.

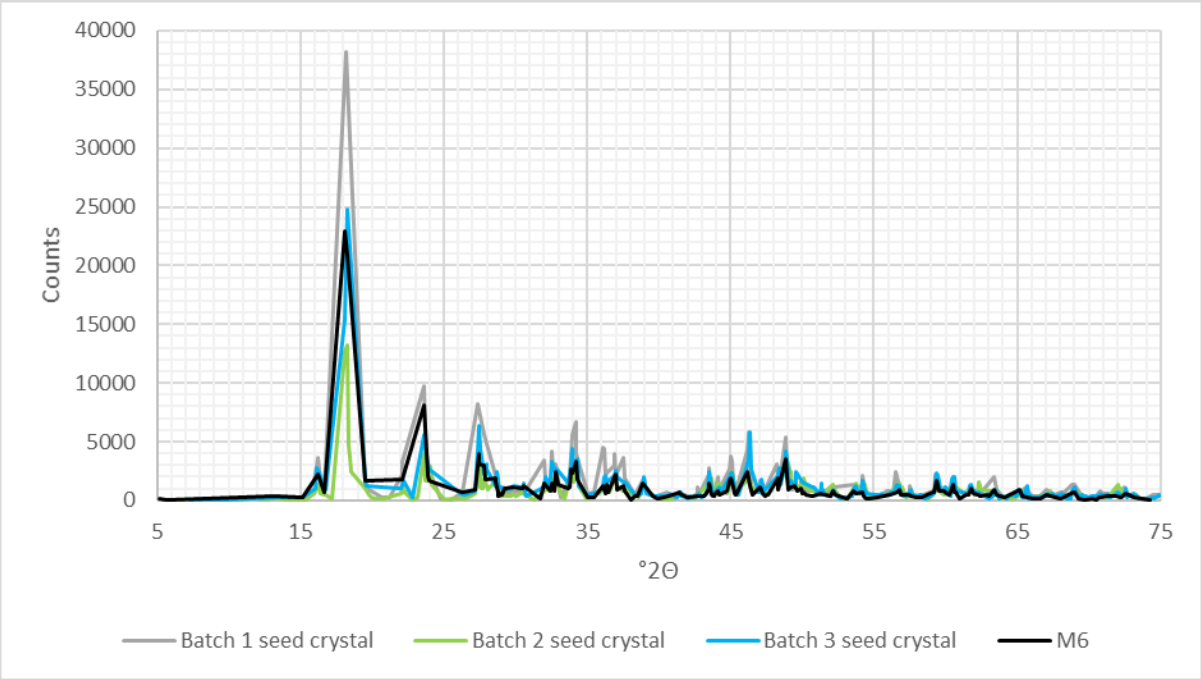

Figure 16. XRD spectra of three different batches of melanterite seed crystals and M6. These four profiles are closely matched to each other and those of melanterite reference spectra.

The samples from M5 and M7 (Fig. 17) are different from the other melanterites. Although they largely match each other, M7 has additional peaks at 18.1, 23.6, and 27.2°2Θ, which correspond to those of melanterite. Also, M7's main peaks are of a lower magnitude than those of M5. This suggests that the M7 sample is of a mixed composition. The reference spectra confirmed this, with M7 matching the patterns of rozenite, szomolnokite ($FeSO_4 \cdot H_2O$), and melanterite, whereas M5 matched only with rozenite.

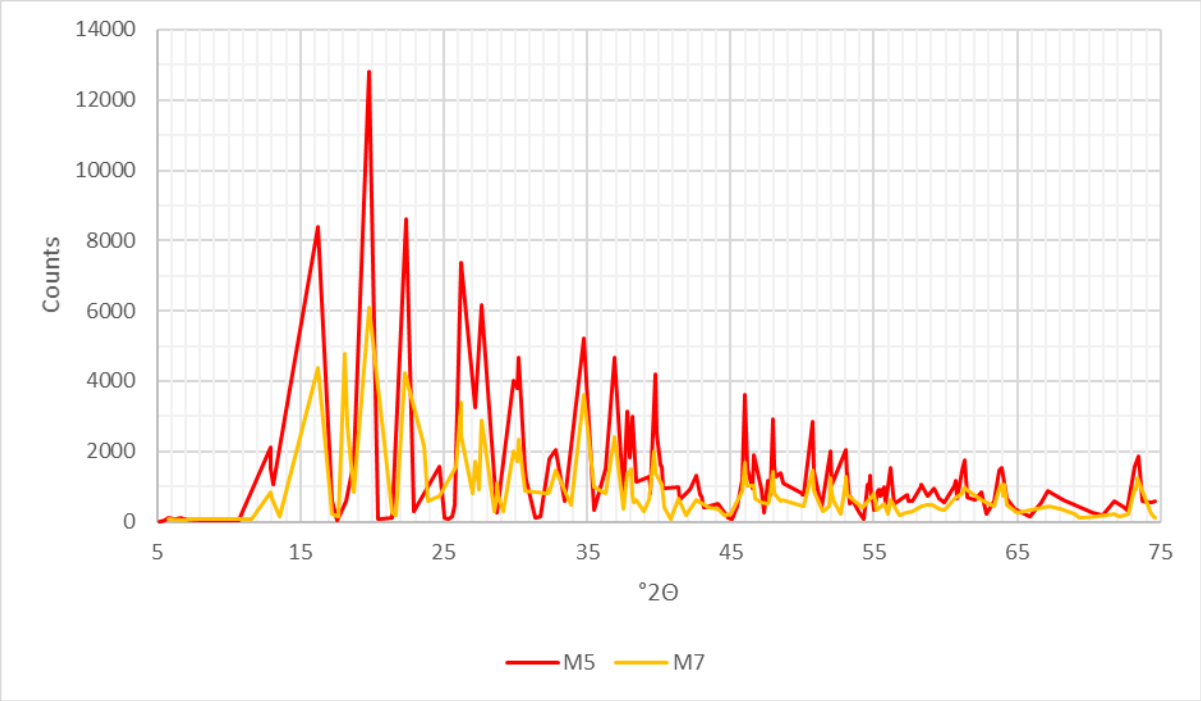

Figure 17. XRD spectra of M5 and M7. Whilst appearing similar, M7 has additional peaks which correspond to melanterite and szomolnokite. M5 and many of M7's peaks correspond to rozenite.

Museum specimens

Four chalcanthites, one pisanite (i.e. cuprian melanterite), and two melanterites were sampled and examined to determine the dehydration products present (Table 5). All resultant spectra are well-matched to the reference patterns.

Table 5. XRD results of NMC museum specimens. Samples 3656, 3686, and 3687 came from different stalactites of the same specimen. Samples 3689 and 3690 came from differently coloured areas of the same specimen. Minerals listed as melanterite are stalactitic in form.

Sample #	Accession #	Listed Mineral	XRD Results	Sample Colour
3654	83.41G.M8476	chalcanthite	siderotil & melanterite	pale blue
3655	83.41G.M8504	pisanite	szomolnokite, siderotil, melanterite	pale orange, pale blue
3656	26.157.GR1	melanterite	hexahydrite, epsomite, jurbanite	white
3684	26.151.GR_	melanterite	kieserite, hexahydrite	white
3685	83.41G.M8482	chalcanthite	szomolnokite	sandy orange
3686	26.157.GR1	melanterite	hexahydrite, epsomite	grey, yellow, & white
3687	26.157.GR1	melanterite	hexahydrite, epsomite	light yellow, white
3688	83.41G.M8481	chalcanthite	siderotil	pale blue
3689	83.41G.M8479	chalcanthite	kieserite, siderotil, melanterite	pale orange
3690	83.41G.M8479	chalcanthite	siderotil, melanterite	pale blue

From the above results, one can conclude:

- The specimens listed as chalcanthite or pisanite were likely originally copper-rich (cuprian) melanterites.
- The stalactitic melanterites are misidentified hydrated magnesium sulphates. These are fairly well-preserved, as they are higher hydrates.

Samples 3654 and 3690 are well matched with each other and to 3688 (Fig. 18), confirming the presence of siderotil ($FeSO_4 \cdot 5H_2O$). The slight variations between 3654 and 3690 can be attributed to different siderotil to melanterite ratios. Most of the peaks of 3655 and 3689 also match those of siderotil and melanterite, chiefly the main ones at 15.9, 18.1, 23.5, 25.8, 27.7, and 33.4°2Θ. However, samples 3656 and 3689 contain additional peaks attributed to szomolnokite and kieserite ($MgSO_4 \cdot H_2O$), respectively. They share three notable peaks at 26.2, 29.2, and 35.6°2Θ, which can be attributed to both of these minerals. A review of the lower magnitude peaks enables their differentiation.

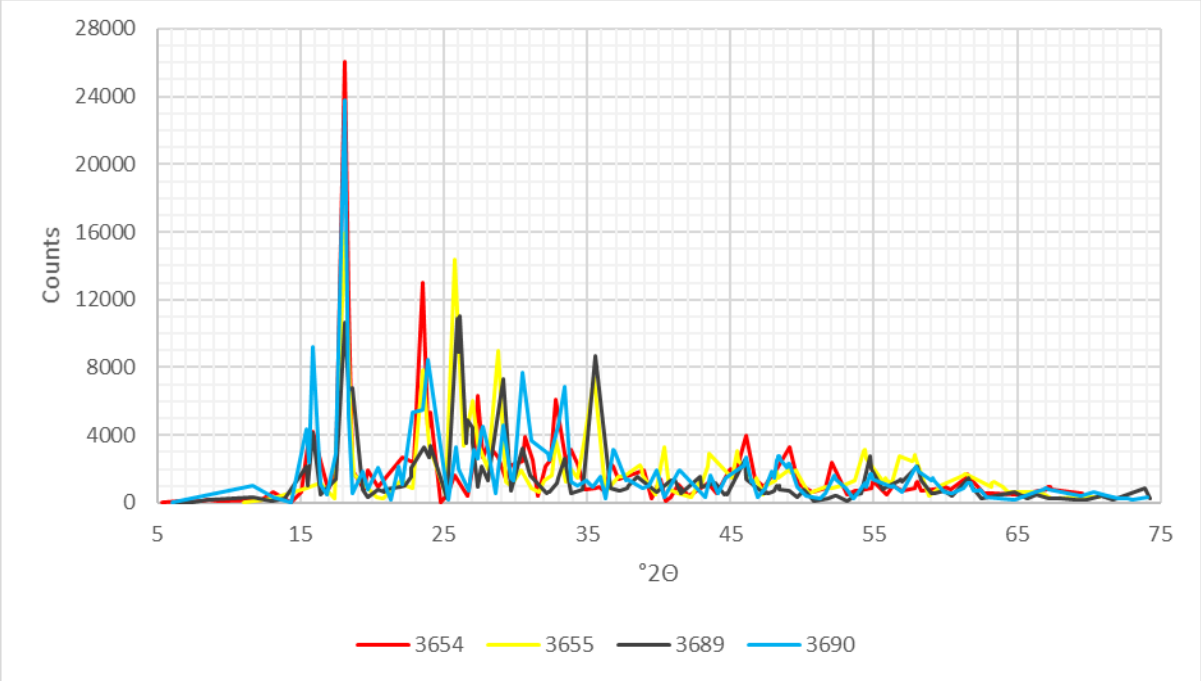

Figure 18. XRD spectra of siderotil and melanterite-containing samples: 3654, 3655, 3689, and 3690. 3654 and 3690 match each other closely and are composed of only siderotil and melanterite. 3655 also contains szomolnokite, whilst 3689 contains kieserite.

A review of the lower magnitude peaks attributed to kieserite was performed, as it occurs in sample 3684 as well (Fig. 19). Only a handful of peaks correspond between these two samples, but they are perfectly so. The main peaks for kieserite are located at 18.5, 26.2, 29.2, 35.6, 54.7, 58.1, 61.6°2Θ, and have been confirmed by the reference patterns.

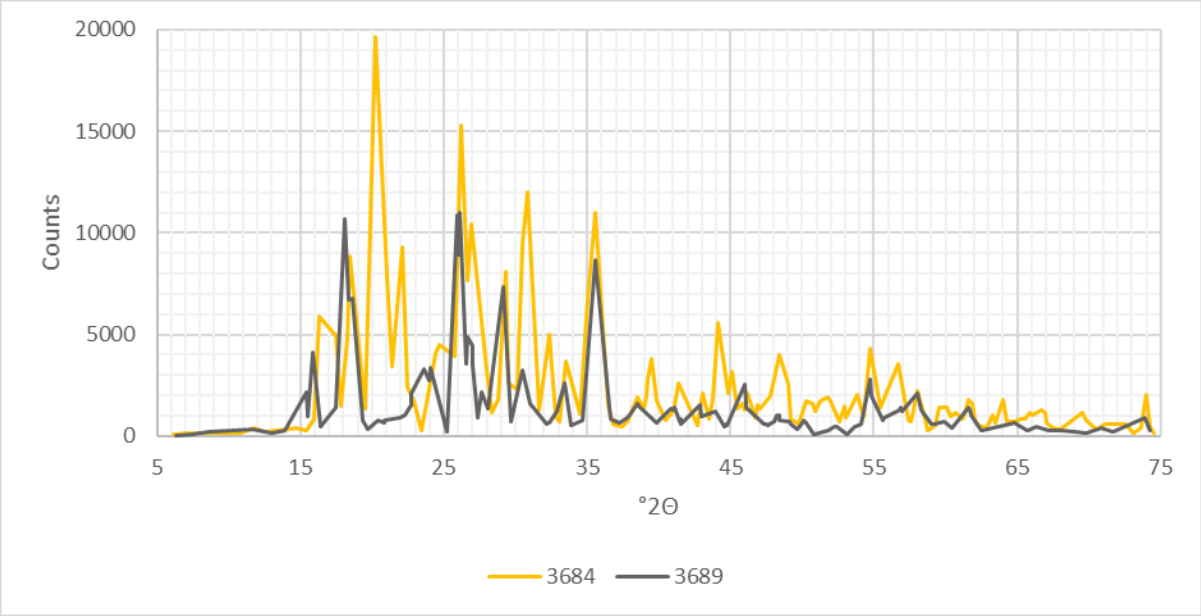

Figure 19. XRD spectra of kieserite-containing samples, 3684 and 3689. While both contain other minerals, seven perfectly matched peaks have been attributed to kieserite.

The additional peaks in 3684's spectra are attributed to hexahydrite ($MgSO_4 \cdot 6H_2O$). The main hexahydrite peaks are located at 16.3, 20.2, 22.0, and 31.0°2Θ. The other three samples (3565, 3686, and 3687; Fig. 20) containing hexahydrite are also associated with epsomite ($MgSO_4 \cdot 7H_2O$), which has greater magnitude peak at 33.4°2Θ.

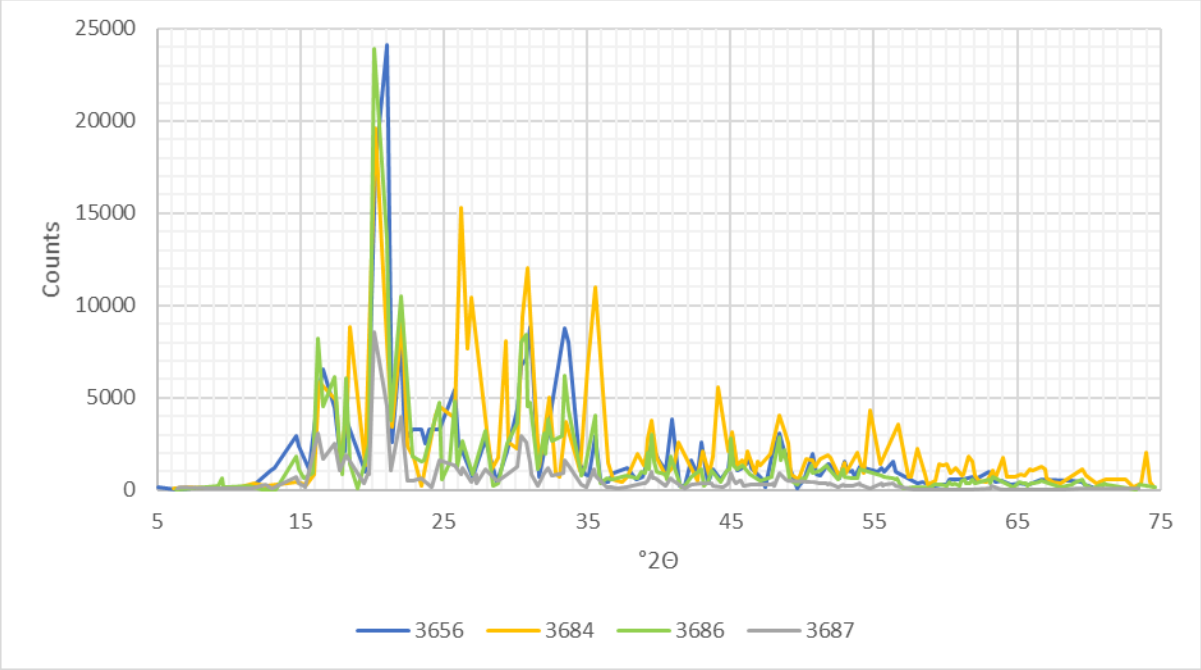

Figure 20. XRD spectra of hexahydrite-containing samples: 3656, 3584, 3686, and 3687. All save for 3684 also contain epsomite and share a well-matched pattern.

FT-IR

The same powdered samples used for XRD (Table 4) were analysed by FT-IR and the resultant spectra were compared to those recorded in the literature.

There is a good correlation between the chalcanthite spectra (Fig. 21), to both each other and the literature (Makreski *et al.* 2005, Bissengaliyeva *et al.* 2016, 2017). All share a strong, sharp peak at 1075-1067cm^{-1}, with a shoulder at 982cm^{-1}, attributed to the stretching modes of SO_4^{2-}($v_{3,1}$). Additional SO_4^{2-} peaks are found at 671-606cm^{-1} (v_4). Chalcanthite's water stretching mode is present as a broad, medium-intensity band with multiple peaks at 3480-2890cm^{-1}. The double peak at 1673-1628cm^{-1} is associated with water's bending mode, whilst the one at 866cm^{-1} is attributed to its deformation. The remaining peaks below 580cm^{-1} are associated with the vibrations of the Cu-O ligand.

The melanterite spectra (Fig. 22) share many of the same peaks as chalcanthite, yet notably lacks the one at 866cm^{-1} attributed to water's deformation. This is most likely due to the different configuration of water within melanterite's structure from having additional water molecules compared to chalcanthite. There is also a difference in the peak positions below 580cm^{-1}, attributed to the shift in frequency that occurs with changes to the metal cation.

All melanterite spectra match those in the literature (Gadsden 1975, Reddy *et al.* 2001, Majzlan *et al.* 2011). M5 (Fig. 22b), however, shows partial resolution of the water stretching peaks and slight shifts in peak positions, which indicates changes to the mineral structure (Gadsden 1975, Salisbury et al. 1991, Socrates 2001). Yet a review of the limited FT-IR data (Majzlan *et al.* 2011, Buzatu *et al.* 2012) for rozenite proves to be a poor match as well. Thus, M5's exact composition cannot be defined with certainty by its FT-IR spectra alone.

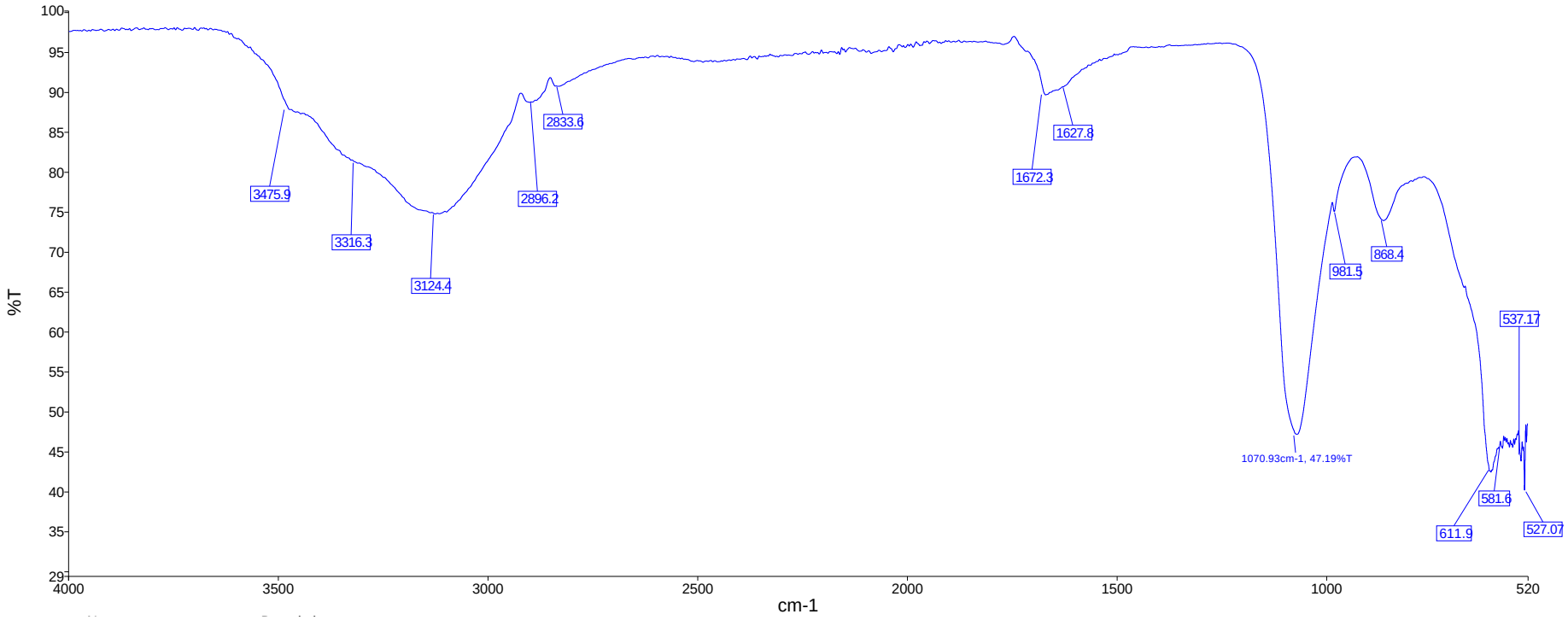

Figure 21. A characteristic chalcanthite FT-IR spectra from C2.

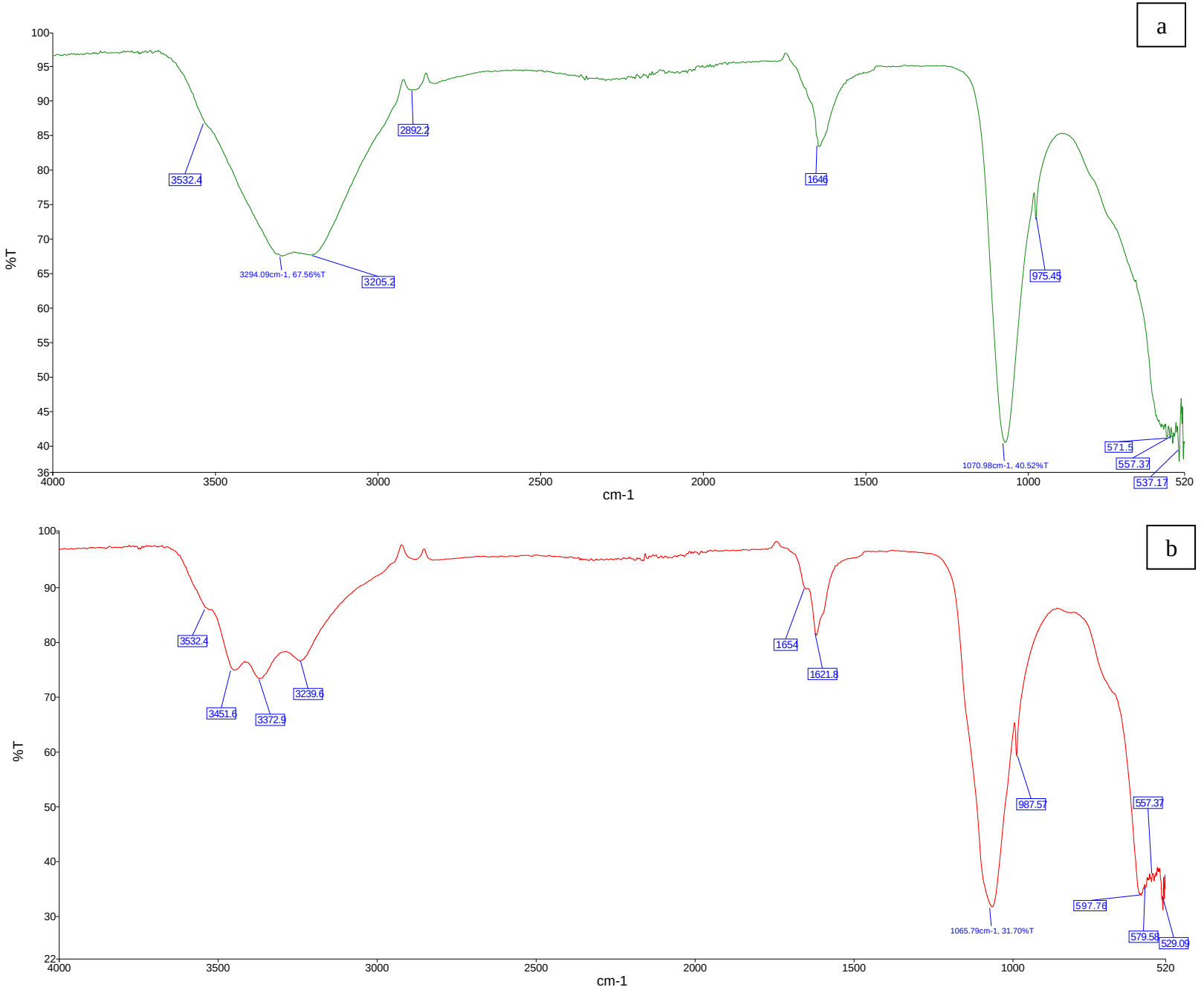

Figure 22. FT-IR spectra from a.) M6 and b.) M5. M6 presents a characteristic melanterite spectra; M5's depicts some deviations, most notably the resolution of water stretching peaks and slight peak shifts.

Raman

The same powder samples used for XRD (Table 4) were also analysed by Raman spectroscopy. The resultant spectra were then compared to those presented in literature.

The spectra of the four chalcanthite samples (Fig. 23) are well-matched amongst each other, with the most notable difference being scales of magnitude. This can be attributed to slight variations in the amount of sample hit by the laser beam. The near-perfect agreement of the spectra suggests that the samples exposed to experimental conditions were minimally affected. This is confirmed by good alignment with the spectra reported in the literature (Berger 1976, Liu and Ullman 1991, Hayez *et al.* 2004, Fu *et al.* 2012, Bissengaliyeva *et al.* 2016).

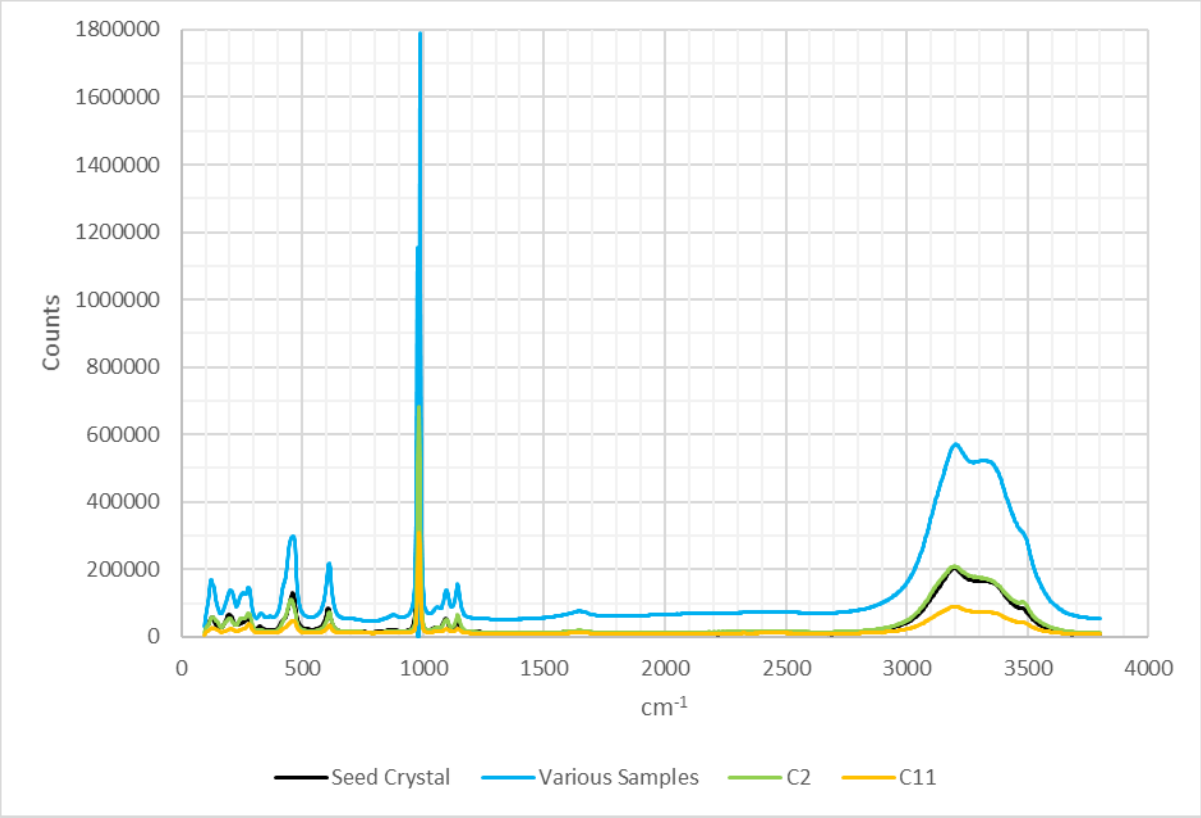

Figure 23. Well-aligned Raman spectra for chalcanthite samples, control, and seed crystal.

All four samples share the strong, sharp peak at 979-987cm^{-1} attributed to the symmetric stretching of SO_4^{2-}(v_1). The other vibrational modes for SO_4^{2-} lie at 1055-1144cm^{-1} (antisymmetric stretch, v_3), 607-613cm^{-1} (antisymmetric bend, v_4), and 417-465cm^{-1} (symmetric bend, v_2). Water's stretching mode is shown as a broad, multi-peaked band at 2900-3600cm^{-1}. Its bending and liberation bands are located at 1642-1654cm^{-1} and 875cm^{-1} respectively, as very weak peaks. The peaks at 199-330cm^{-1} are attributed to the Cu-O ligand vibrations, and those below 160cm^{-1} are associated with the crystal's lattice vibrations.

Similar peak positions are presented by the melanterite spectra (Fig. 24), with the primary variation being the relationship between the SO_4^{2-}(v_1) and water stretching bands. This is attributed to melanterite's different structure induced by higher hydration and the iron cation.

The relationship between the heights of the SO_4^{2-}(v_1) and water stretching bands is greater for melanterite than it is for chalcanthite. The peak height for chalcanthite's water

stretch is about 30% the height of the $SO_4^{2-}(v_1)$ peak, whereas it is approximately 50% for both melanterite and rozenite. This suggests a different relationship between the metal cations and their bound waters. This is further evidenced in the relative shift in the position of melanterite's water stretching band. Its increased distance from the $SO_4^{2-}(v_1)$ peak indicates weaker hydrogen bonds within the molecule, meaning that they are easier to break, liberating the water. Therefore, dehydration occurs more readily in melanterite and rozenite than in chalcanthite.

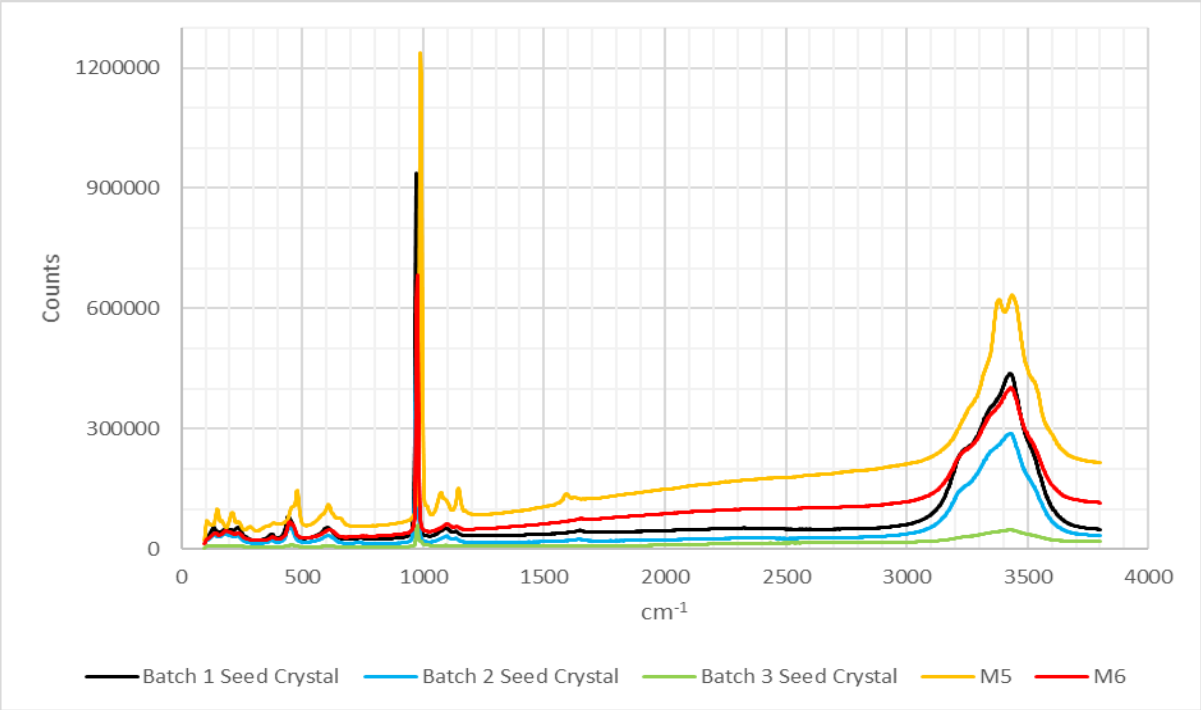

Figure 24. Raman spectra for the three batches of melanterite seed crystals, M5, and M6. All save for M5 are in good agreement with each other and are attributed as melanterite. M5, on the other hand, displays additional peaks and slight shifts in peak positions in line with the spectra for rozenite.

The melanterite spectra are consistent with each other, save for that of M5, which has additional peaks and slight shifts in peak position. M5 also has a narrower water stretching band, evidencing that it contains less water than the other samples. These variations are in line with the spectra for rozenite (Chio *et al.* 2005, 2007, Apopei *et al.* 2014, Buzatu *et al.* 2016). The other four spectra are in good agreement with those for melanterite (Chio *et al.* 2005, 2007, Majzlan *et al.* 2011, Apopei *et al.* 2014, Buzatu *et al.* 2016).

Discussion

While the chalcanthite samples experienced some water loss (identified by weight measurements), the dehydration of melanterite samples was on a far greater scale, detectable visually and by all analytical methods used. Yet only XRD and Raman spectroscopy successfully identified the dehydration product as rozenite. Szomolnokite was also identified as an additional product by XRD. It is attributed to a second phase dehydration product that began to form atop rozenite. Had the samples been exposed for a longer period of time, it is likely that szomolnokite would have become the primary phase, as it is stable below 30%RH (Waller 1992, Blount 1993). This evidences the need for strict environmental control for melanterite and rozenite specimens.

Chalcanthite, on the other hand, is largely stable within a wide range of museum conditions (Fig. 1). This experiment showed that pure chalcanthite can even be stable in conditions just past its equilibrium curve. It is likely in this case that the samples had not experienced conditions sufficiently past those required to overcome the activation energy barrier required for a phase transition. But that is not to say that such conditions do not exist in museums. Thus, chalcanthite should still be listed as susceptible for dry (generally <35%RH) conditions. Cuprian melanterite should be treated as melanterite rather than chalcanthite, due to its iron content inducing environmental instability.

It is inconclusive whether synthetic crystals present changes similar to those of museum specimens. As outlined in Table 5, many of the specimens were misidentified at accession. As of yet, no dehydrated chalcanthite or melanterite specimen has been found and analysed with XRD at NMC to confirm their dehydration products.

Cuprian melanterite cannot be used to anticipate the dehydration products of either chalcanthite or melanterite. Firstly, it likely does not contain enough copper to form copper sulphates. Secondly, the presence of copper influences the level of hydration through the stabilisation of the siderotil structure (Peterson and Grant 2005) rather than that of rozenite. However, it is likely that rozenite is the primary dehydration product of melanterite, as it has been observed both within museums (Wiese *et al.* 1987, Blount 1993, Odin *et al.* 2015) and mines (Nordstrom and Alpers 1999, Jambor *et al.* 2000, Hammarstrom *et al.* 2005, Apopei *et al.* 2014, Buzatu *et al.* 2016). As for chalcanthite, it is possible that purer samples do not undergo sufficient dehydration to produce a change in hydration state, as NMC does hold some exceptional chalcanthite specimens which still look fresh.

Assessment of Analytical Techniques for Museum Use

While all analytical methods proved effective in identifying physical and chemical changes that occurred to the studied minerals, they are not equally applicable for museum use (Table 6).

The ideal technique is one that is accessible, cost effective, quick, straightforward, and requires little to no sampling. These criteria are critical when assessing large collections but may be compromised for high value or priority collections or when answering specific research questions. Of the methods used, photography, colorimetry, XRD, FT-IR, and Raman spectroscopy would be the most practical methods to employ within a museum setting. However, each technique has its own limitations. Photography and colorimetry require some methodological and technical refinements to optimise their use, and the three spectroscopic techniques are not necessarily standalone methods and the requisite sampling may not always be possible for certain mineral specimens.

Weighing samples is a quick and easy way to determine if damage has occurred. However, contextual evidence and further forms of analysis are needed to identify the type and extent of damage. It is unlikely to be adopted within museums, due to the time commitment required to regularly weigh thousands of specimens.

Colorimetry is likewise an easy, useful method to quantify changes to colour, an important physical feature of minerals. It is beneficial to have such a method available for museums, as one may not remember a specimen's original appearance, staff may change, and photography can be unreliable, due to colour variation created by different lighting. Yet, there are some drawbacks to this technique. Firstly, the technique requires knowledge of colour

Table 6. A qualitative assessment of the practicality of employing various analytical techniques for monitoring mineralogical collections within a museum setting, where 0: no/none; 1: minimal (<5min); 2: some (<30min); 3: yes/extensive (>30min). Assigned values can vary depending on the specific application of each method.

	Identification	Monitoring	Access	$\frac{\text{Time}}{\text{Sample}}$	Cost Effective	Sampling Required	Knowledge Required	Standalone Method	Practicality
Weight Measurements	0	2	3	1	3	0	1	0	1
Colorimetry	0	2	2	1	3	0	2	3	2
Photography	0	3	3	1-3	1-3	0	1-2	3	3
CT	0	2	1	3	1	0-2	2	2	1
X-radiography	0	2	1	2	1	0-2	2	1	1
SEM	2	0	2	3	1	0-2	2	1	1
EDX	3	3	1	1	1	0-2	2	0	1
XRD	3	3	2	2	2	1	2-3	2	2
FT-IR	3	3	2-3	1	3	1	1-2	2	3
Raman	3	3	1-2	2	2	1	1-2	2	2

science to fully analyse and interpret the data. Secondly, current models of colorimeters and spectrophotometers are ill-designed to be used with minerals. In addition to being blocky, the smallest reading aperture (3mm) is often too large for many mineral surfaces. Thus, anything small, uneven, or with protrusions is difficult to measure. Additional light passed through transparent or translucent minerals can skew the data as well. Thus, refinements are necessary to produce reliable, reproducible results.

Photography is a very flexible technique that can meet various demands. If a visual record is all that is needed, any decent camera, ruler, and colour card will do. However, if detailed comparisons or measurements are required, a higher-spec camera should be used to improve image quality. With such applications, additional equipment—such as lights, mounts, and backdrops—is often needed to produce replicable conditions. But even then, images of the same specimen from different photoshoots may not be directly comparable if the specimen is not positioned exactly as before. Thus, methodological consistency is needed to effectively capture and compare micro-effects (ex. slight colour change, crack propagation) for collection monitoring. However, mid-grade cameras can be used to produce acceptable results for museum records and the monitoring of macro-effects (ex. noticeable discolouration, efflorescence, spalling).

While x-ray machines can be found within the museum sector—due to its use in other conservation areas—there is little practicality in using the technique without a research question in mind. With CT, however, the addition of a 3D model—in conjunction with the 2D slices—has greater promise and applications within museums, especially as the technology improves and becomes more accessible.

There is also questionable applicability of using an SEM to view minerals due to the forced vacuum. An alternative would be to use an environmental scanning electron microscope (ESEM), as it retains atmospheric pressure and moisture. However, there is less access to these than SEMs, especially for museums, due to the availability and cost of the equipment.

EDX equipment is often coupled with an SEM or a transmission electron microscope (TEM), rather than being a standalone device, greatly restricting access to this analytical technique. However, x-ray fluorescence (XRF) can also be used to identify elemental composition. If able to produce similar or better results than EDX, XRF would be the method preferred by museums due to its wider availability and non-destructivity. The only difference between the two is that EDX can focus on localised, microscopic areas of a surface, which is useful for the identification of efflorescence and reaction products. This discrimination may not be feasible with an XRF due to its larger detection area.

XRD is a standard, critical technique in mineralogy. While XRD can act as a standalone technique, it is not necessarily so. If one does not have an idea of what to anticipate, a form of elemental or compositional analysis is critical to successfully narrow down the comparative results. Some knowledge of mineral paragenesis and locality is also useful when identifying a species within mixed-composition samples.

There has been increasing access to both FT-IR and Raman spectroscopy within museums as the equipment improves and becomes less expensive. The former is readily available and frequently used within the sector. The latter less so, due to Raman generally being more costly and requiring more knowledge of the technique. This may make access troublesome. Yet both of these methods are suitable in identifying composition and structure. When applied to minerals, one must run below 600cm^{-1} to successfully identify the species. If not, usually the peaks will only correspond with water and the cation. The only drawback to

both methods is the lack of published mineral spectra, especially for FT-IR, to aid identification.

Areas for Further Research

This experiment exposed many areas of further experimentation which may be useful for the study and monitoring of mineral specimens. Firstly, a study comparing the surface appearance of hydrated and dehydrated minerals under an ESEM to an SEM would prove useful in determining differences between cracking patterns displayed within and without a vacuum. Secondly, an assessment of the usability and applicability of XRF for mineral collections—compared to EDX—could add another analytical technique to the arsenal. A study of the rehydration of once hydrated minerals, to determine if it is possible to reverse the effects of short-term dehydration, could become a treatment method if successful. And lastly, a longer experiment observing the efficacy of Parafilm as a long-term moisture barrier may have implications for the storage of environmentally sensitive materials.

Conclusion

Dehydrating samples of chalcanthite and melanterite did produce detectable physicochemical changes. When compared to the examined museum specimen, it is inconclusive whether synthetic crystals present changes similar to natural ones. Chalcanthite experienced very little change, only evidenced by weight measurements. Melanterite, on the other hand, underwent sufficient dehydration to alter into a lower hydrate, which was detected by all forms of analysis, warranting their use in research applications. Only a few techniques—photography, colorimetry, XRD, FT-IR, and Raman spectroscopy— are pragmatic for museum applications at present. Additional research may add further techniques to this list and provide new methods to successfully preserve instable mineral specimens.

Acknowledgements

I would like to thank the following people for sharing their expertise, knowledge, equipment, advice, and support throughout this experiment. Without their assistance, this experiment would not have been completed in full.

- Dr. Heather Viles, University of Oxford
- Dr. Josep Grau-Bové, University College London
- James Appleby, Robert Wells, and James Earl, OR3D
- Dr. Christian Baars, Dr. Jana Horak, Tom Cotterell, and Amanda Valentine-Baars, National Museum Cardiff
- David Howell, Weston Library, University of Oxford
- Professor Tony Parker, Rutherford-Appleton Laboratory
- Chris Doherty, University of Oxford
- Dr. Leonard Schronk and Dr. Karen Hyver

References

Apopei, A.I., Buzgar, N., Damian, G., and Buzatu, A., 2014. The Raman study of weathering minerals from the Coranda-Hondol open pit (Certej gold-silver deposit) and their photochemical degradation products under laser irradiation. *Canadian Mineralogist*, 52 (6), 1027–1038.

Berger, J., 1976. Infrared and Raman spectra of CuSO4*5H2O, CuSO4*5D2O, and CuSeO4*5H2O. *Journal of Raman Spectroscopy*, 5, 103–144.

Bissengaliyeva, M., Ogorodova, L., Vigasina, M., Mel'Chakova, L., Kosova, D., Bryzgalov, I., and Ksenofontov, D., 2016. Enthalpy of formation of natural hydrous copper sulfate: Chalcanthite. *Journal of Chemical Thermodynamics*, 95, 142–148.

Bissengaliyeva, M.R., Bekturganov, N.S., Gogol, D.B., and Taimassova, S.T., 2017. Low-temperature heat capacity and thermodynamic functions of natural chalcanthite. *Journal of Chemical Thermodynamics*, 111, 199–206.

Blount, A.M., 1993. Nature of the alterations which form on pyrite and marcasite during collection storage. *Collection Forum*, 9 (1), 1–16.

Buzatu, A., Dill, H.G., Buzgar, N., Damian, G., Maftei, A.E., and Apopei, A.I., 2016. Efflorescent sulfates from Baia Sprie mining area (Romania) - Acid mine drainage and climatological approach. *Science of the Total Environment*, 542, 629–641.

Chio, C.H., Sharma, S.K., and Muenow, D.W., 2005. Micro-Raman studies of hydrous ferrous sulfates and jarosites. *Spectrochimica Acta - Part A: Molecular and Biomolecular Spectroscopy*, 61 (10), 2428–2433.

Chio, C.H., Sharma, S.K., and Muenow, D.W., 2007. The hydrates and deuterates of ferrous sulfate (FeSO4): a Raman spectroscopic study. *Journal of Raman Spectroscopy*, 38, 87–99.

Chou, I.M., Seal, I.R., and Hemingway, B.S., 2002. Determination of melanterite-rozenite and chalcanthite-bonattite equilibria by humidity measurements at 0.1 MPa. *American Mineralogist*, 87 (1), 108–114.

Chou, I.M., Seal, R.R., and Wang, A., 2013. The stability of sulfate and hydrated sulfate minerals near ambient conditions and their significance in environmental and planetary sciences. *Journal of Asian Earth Sciences*, 62, 734–758.

Cotterell, T. 2019. *Discussion on the value of minerals.* [conversation] (Personal communication, 19 July 2019).

Fu, X., Yang, G., Sun, J., and Zhou, J., 2012. Vibrational spectra of copper sulfate hydrates investigated with low-temperature raman spectroscopy and terahertz time domain spectroscopy. *Journal of Physical Chemistry A*, 116 (27), 7314–7318.

Gadsden, J. A. 1975. *Infrared Spectra of Minerals and Related Inorganic Compounds*. London: Butterworths & Co. Ltd.

Hammarstrom, J.M., Seal, R.R., Meier, A.L., and Kornfeld, J.M., 2005. Secondary sulfate minerals associated with acid drainage in the eastern US: Recycling of metals and acidity in surficial environments. *Chemical Geology*, 215 (1-4 SPEC. ISS.), 407–431.

Hayez, V., Guillaume, J., Hubin, A., and Terryn, H., 2004. Micro-Raman spectroscopy for the study of corrosion products on copper alloys: setting up of a reference database and studying works of art. *Journal of Raman Spectroscopy*, 35 (89), 732–738.

Jambor, J.L., Nordstrom, D.K., and Alpers, C.N., 2000. Metal-sulfate Salts from Sulfide Mineral Oxidation. *In*: C.N. Alpers, J.L. Jambor, and D.K. Nordstrom, eds. *Sulfate Minerals: Crystallography, Geochemistry, and Envrionmental Significance*. Washington D.C.: Mineralogical Society of America, 303–350.

Johnston-Feller, R., 2001. *Color Science in the Examination of Museum Objects: Nondestructive Procedures*. Los Angeles: Getty Publications.

Konica Minolta, 2007. *Precise color communication: color control from perception to instrumentation*. Konica Minolta Sensing.

Konica Minolta, 2019. Specular Component Included (SCI) vs. Specular Component Excluded (SCE) [online]. Available from: https://sensing.konicaminolta.us/blog/specular-component-included-sci-vs-specular-component-excluded-sce/ [Accessed 9 Jan 2019].

Liu, D. and Ullman, F.G., 1991. Raman spectrum of CuSO4 · 5H2O single crystal. *Journal of Raman Spectroscopy*, 22 (9), 525–528.

Majzlan, J., Alpers, C.N., Koch, C.B., McCleskey, R.B., Myneni, S.C.B., and Neil, J.M., 2011. Vibrational, X-ray absorption, and Mössbauer spectra of sulfate minerals from the weathered massive sulfide deposit at Iron Mountain, California. *Chemical Geology*, 284 (3–4), 296–305.

Makreski, P., Jovanovski, G., and Dimitrovska, S., 2005. Minerals from Macedonia: XIV. Identification of some sulfate minerals by vibrational (infrared and Raman) spectroscopy. *Vibrational Spectroscopy*, 39 (2), 229–239.

Nordstrom, D.K. and Alpers, C.N., 1999. Geochemistry of acid mine waters. *The Environmental Geochemistry of Mineral Deposits, Part A: process techniques and health issues*, 6 (October), 133–160.

Odin, G.P., Vanmeert, F., Farges, F., Gand, G., Janssens, K., Romero-Sarmiento, M.F., Steyer, J.S., Vantelon, D., and Rouchon, V., 2015. Alteration of fossil-bearing shale (Autun, France; Permian), part II: Monitoring artificial and natural ageing by combined use of S and Ca K-edge XANES analysis, Rock-Eval pyrolysis and FTIR analysis. *Annales de Paleontologie*, 101 (3), 225–239.

Peterson, R.C. and Grant, A.H., 2005. Dehydration and crystallization reactions of secondary sulfate minerals found in mine waste: In situ powder-diffraction experiments. *Canadian Mineralogist*, 43 (4), 1171–1181.

Reddy, S.N., Rao, P.S., Ravikumar, R.V.S.S.N., Reddy, B.J., and Reddy, Y.P., 2001. Spectral investigations on melanterite mineral from France. *Spectrochimica Acta - Part A Molecular and Biomolecular Spectroscopy*, 57 (6), 1283–1287.

Salisbury, J.W., Walter, L.S., Vergo, N., and D'Aria D.M. 1991. *Infrared (2.1-25μm) Spectra of Minerals*. Baltimore: Johns Hopkins University Press

Socrates, G. 2001. *Infrared and Raman Characteristic Group Frequencies: Tables and Charts*. 3rd ed. Chichester: John Wiley & Sons, Ltd.

Waller, R., 1992. Temperature- and humidty-sensitive mineralogical and petrological specimens. *In*: F.M. Howie, ed. *The Care and Conservation of Geological Materials: Minerals, Rocks, Meteorites and Lunar Finds*. Oxford: Butterworth-Heinemann, 25–50.

Wiese, R.G., Powell, M.A., and Fyfe, W.S., 1987. Spontaneous formation of hydrated iron sulfates on laboratory samples of pyrite- and marcasite-bearing coals. *Chemical Geology*, 63 (1–2), 29–38.

Appendix A. Mineralogy and Growth Procedures

Table 7. Mineralogical data for chalcanthite and melanterite

	Chalcanthite	Melanterite
Chemical Formula	$CuSO_4 \cdot 5H_2O$	$FeSO_4 \cdot 7H_2O$
Crystal System	Triclinic	Monoclinic
Morphology	Prismatic crystals, stalactitic, veins, or granular masses	Stalactitic, veins, or granular masses; large crystals are rare
Appearance	Translucent; pale–dark blue	Translucent; glass green or aqua
Hardness (Moh's)	2.5	2
Specific Gravity	2.29	1.89

Chalcanthite

1. Heat deionized water to approximately 70°C to aid dissolution
2. Create a super-saturated solution with 1-part copper(II) sulphate and 2-parts deionized water, mixing well
3. Decant the solution into a container so that 1-2cm is standing
4. Allow the solution to evaporate overnight and produce seed crystals
5. Remove seed crystals from any remaining solution and tie cotton thread around them
6. Decant fresh super-saturated solution into a container so that the crystal is entirely submerged without touching the base of the container
7. Submerge the seed crystal into solution, suspended from a rod resting on the container's mouth
8. Let evaporate
9. Repeat 6-8 until crystal is of desired size

Melanterite

1. Heat deionized water to approximately 55°C to aid dissolution
2. Create a super-saturated solution with 1-part iron(II) sulphate and 1-part deionized water, mixing well
3. Filter the solution to remove any iron oxide precipitant that is immediately produced
4. Add 0.2N sulphuric acid – approximately 25ml acid to 100ml solution – and mix well
5. Decant some solution into a container so that 1-2cm is standing
6. Allow to evaporate for up to two days in order to produce seed crystals
7. Remove seed crystals from solution
8. Decant fresh super-saturated solution into another container so that the crystal is submerged with excess
9. Add the seed crystal to solution, letting it rest at the bottom of the container
10. Let evaporate
11. Repeat 8-10 until crystal is of desired size

Caution is needed when adding sulphuric acid to the melanterite solution. Too much will dilute the solution, inhibiting crystallization or producing small crystals. The solution also requires filtering every so often to remove iron oxide precipitants that form after extended periods of evaporation.

The colour of the melanterite solution does not seem to be an indicator of a 'good' solution. Aqua or green is not better than olive or yellow. In fact, the converse seems to be true; an aqua solution is likely too dilute. Melanterite crystals can still grow from an orange solution, but there is a higher risk of an iron oxide precipitant to form and be included in the crystals. Olive seems to be the desired colour. The one thing colour *does* indicate, however, is the colour of the crystals themselves. A greener solution will produce aqua crystals whereas an orange/yellower solution will produce green crystals. These both are acceptable colours for melanterite, and FT-IR, Raman, and XRD analysis proves there is little variation amongst them.

Allowing the melanterite crystals to form at the bottom of the container seemed to create larger crystals, whereas with suspension, either a series of small crystals or a mass of fine crystals would form. This is likely due to melanterite having a growth rate that is slower than that of evaporation.

Residual solutions and any unwanted crystalline material can be reused by following the steps to make a super-saturated solution. For melanterite solutions, additional sulphuric acid will be needed.

Appendix B. Colorimetry Data

These values, in addition to ΔE^*_{ab}, were calculated by Konica Minolta's SpectraMagic NX software from the specular data captured by the spectrophotometer.

Table 8. Colorimetry data (L, a*, b*, C*, and h) for the melanterite minerals before and after dehydration, as well as the change between these values. Ranges, means, and standard deviations are also provided.*

Melanterite SCE Before		L*(D65)	a*(D65)	b*(D65)	C*(D65)	h(D65)
Sample Number	M1	31.22	-5.16	7.68	9.25	123.91
	M2	33.19	-5.62	8.25	9.98	124.28
	M3	32.50	-4.30	11.15	11.95	111.09
	M4	30.35	-12.86	5.76	14.09	155.85
	M5	38.59	-11.43	3.92	12.08	161.09
	M6	51.10	-10.21	2.64	10.55	165.52
	M7	30.01	-10.63	4.45	11.53	157.27
	M8	36.66	-16.74	4.29	17.28	165.62
	M9	37.30	-10.83	5.37	12.09	153.63
	Range	21.09	12.44	8.51	8.03	54.53
	Mean	35.66	-9.75	5.95	12.09	146.47
	Standard Deviation	6.21	3.82	2.49	2.26	19.59
Melanterite SCE After		L*(D65)	a*(D65)	b*(D65)	C*(D65)	h(D65)
Sample Number	M1	88.40	0.71	18.21	18.22	87.77
	M2	31.99	-4.17	4.97	6.49	129.95
	M3	90.19	-1.01	13.75	13.79	94.21
	M4	34.31	-15.00	5.70	16.05	159.21
	M5	94.76	-2.23	6.15	6.54	109.94
	M6	32.76	-10.73	3.80	11.38	160.49
	M7	92.40	0.21	9.22	9.22	88.72
	M8	32.19	-10.42	5.85	11.94	150.70
	M9	95.18	-3.10	4.65	5.59	123.75
	Range	63.19	15.71	14.41	12.63	72.72
	Mean	65.80	-5.08	8.03	11.02	122.75
	Standard Deviation	29.57	5.27	4.60	4.20	27.78
Melanterite SCE Δ		L*(D65)	a*(D65)	b*(D65)	C*(D65)	H*(D65)
Sample Number	M1	57.18	5.87	10.53	8.97	-8.06
	M2	-1.20	1.46	-3.27	-3.49	0.80
	M3	57.70	3.29	2.60	1.84	-3.77
	M4	3.96	-2.15	-0.07	1.96	0.88
	M5	56.16	9.20	2.23	-5.54	-7.68
	M6	-18.34	-0.52	1.16	0.84	-0.96
	M7	62.39	10.84	4.76	-2.31	-11.61
	M8	-4.47	6.32	1.55	-5.33	-3.73
	M9	57.88	7.73	-0.72	-6.50	-4.24
	Range	80.73	12.99	13.80	15.47	12.49
	Mean	30.14	4.67	2.09	-1.06	-4.26
	Standard Deviation	31.96	4.19	3.67	4.68	3.99

Table 9. Colorimetry data (L, a*, b*, C*, and h) for the chalcanthite minerals before and after dehydration, as well as the change between these values. Ranges, means, and standard deviations are also provided.*

Chalcanthite SCE Before		L*(D65)	a*(D65)	b*(D65)	C*(D65)	h(D65)
Sample Number	C1	29.41	1.47	-18.60	18.65	274.52
	C2	29.06	2.71	-13.93	14.19	281.02
	C3	18.05	2.98	-16.30	16.57	280.35
	C4	15.37	1.96	-12.89	13.04	278.64
	C5	22.94	0.49	-15.49	15.50	271.80
	C6	27.94	2.34	-16.93	17.09	277.85
	C7	11.50	7.54	-21.74	23.01	289.13
	C8	14.08	4.03	-17.82	18.27	282.76
	C9	32.55	0.48	-11.95	11.96	272.30
	C10	25.52	2.54	-16.25	16.45	278.89
	C11	31.50	-1.05	-14.35	14.39	265.83
	C12	27.35	2.34	-15.94	16.11	278.35
	C13	27.70	2.89	-13.83	14.13	281.82
	C14	16.94	0.80	-31.28	31.29	271.47
	C15	34.78	-7.55	-26.97	28.00	254.37
	C16	13.51	4.05	-26.93	27.23	278.55
	C17	11.95	6.67	-24.96	25.83	284.97
	C18	27.68	-1.41	-22.02	22.07	266.33
	C19	16.05	2.67	-24.63	24.78	276.18
	C20	28.36	2.55	-13.43	13.67	280.77
	Range	23.28	15.09	19.33	19.33	34.76
	Mean	22.43	1.91	-19.10	19.41	276.13
	Standard Deviation	7.40	3.02	5.45	5.59	7.57
Chalcanthite SCE After		L*(D65)	a*(D65)	b*(D65)	C*(D65)	h(D65)
Sample Number	C1	19.48	3.93	-19.46	19.86	281.41
	C2	28.09	3.22	-16.04	16.36	281.36
	C3	25.60	-0.14	-14.97	14.97	269.46
	C4	20.15	-0.46	-17.93	17.93	268.54
	C5	18.05	4.33	-20.51	20.96	281.91
	C6	25.45	1.88	-18.86	18.95	275.70
	C7	21.26	2.15	-17.49	17.62	277.02
	C8	20.90	-5.04	-30.46	30.87	260.61
	C9	31.62	-8.68	-28.15	29.46	252.86
	C10	24.08	5.22	-20.04	20.70	284.59
	C11	32.53	-0.54	-15.33	15.34	267.97
	C12	30.02	-3.23	-20.62	20.87	261.10
	C13	25.14	2.04	-12.50	12.66	279.25
	C14	11.30	5.03	-20.86	21.46	283.54
	C15	34.65	-7.76	-26.15	27.28	253.47
	C16	19.05	3.34	-17.81	18.13	280.62
	C17	14.70	6.72	-27.80	28.60	283.59
	C18	35.63	-3.36	-24.57	24.80	262.22
	C19	24.53	1.97	-21.74	21.83	275.17
	C20	16.15	0.32	-31.96	31.96	270.57
	Range	24.33	15.40	19.46	19.30	31.73
	Mean	23.93	0.21	-21.54	21.91	271.57
	Standard Deviation	6.56	4.17	5.25	5.43	9.90
Chalcanthite SCE Δ		L*(D65)	a*(D65)	b*(D65)	C*(D65)	H*(D65)
Sample Number	C1	-9.94	2.46	-0.87	1.20	2.31
	C2	-0.97	0.51	-2.11	2.17	0.09
	C3	7.55	-3.12	1.33	-1.60	-2.99
	C4	4.77	-2.42	-5.04	4.90	-2.69

	C5	-4.89	3.84	-5.02	5.47	3.18
	C6	-2.49	-0.45	-1.93	1.86	-0.68
	C7	9.75	-5.38	4.25	-5.39	-4.25
	C8	6.83	-9.07	-12.64	12.61	-9.13
	C9	-0.94	-9.16	-16.20	17.50	-6.34
	C10	-1.43	2.67	-3.79	4.26	1.84
	C11	1.03	0.50	-0.98	0.95	0.56
	C12	2.67	-5.57	-4.68	4.76	-5.50
	C13	-2.56	-0.86	1.33	-1.47	-0.60
	C14	-5.64	4.22	10.41	-9.83	5.45
	C15	-0.12	-0.22	0.81	-0.72	-0.43
	C16	5.53	-0.71	9.11	-9.10	0.80
	C17	2.75	0.04	-2.84	2.76	-0.66
	C18	7.96	-1.95	-2.55	2.73	-1.68
	C19	8.48	-0.70	2.89	-2.95	-0.41
	C20	-12.21	-2.24	-18.53	18.29	-3.72
	Range	21.96	13.38	28.94	28.12	14.58
	Mean	1.50	-1.70	-2.45	2.50	-1.51
	Standard Deviation	5.96	3.61	7.03	7.16	3.35